Review Article: Modeling Granular Media on the Computer

H. J. Herrmann and S. Luding
Institute for Computer Applications 1,
Pfaffenwaldring 27, D-70569 Stuttgart, GERMANY

March 30, 1998

Abstract

Granular materials, like sand, powder or grains present intriguing phenomena. Vibration and shearing can lead to convective motion and segregation. A variation of stress may cause localization phenomena like stress chains or shear bands. Granular systems are thus in a state far from thermodynamic equilibrium, however, we present an attempt for a thermodynamic description by extending the concept of compactivity.

In vibrating containers under the influence of gravity, the granular material shows a peculiar density profile. In the weak dissipation / strong agitation limit the density decays exponentially with height, whereas one observes an almost uniform profile in the case of strong dissipation / weak agitation. In the latter regime, the formation of convection cells due to walls or amplitude modulations can be observed. The onset of fluidization can be determined and is in good agreement with experiments. Connected to convection is the effect of rapid segregation, however, comparatively slow segregation can also be observed in the absence of convection.

Numerical simulations of flow in hoppers show that the density fluctuations have a power spectrum, allowing for large "events" with finite probability. There is also ample experimental and numerical evidence showing the existence of spontaneous density patterns in granular material flowing through pipes or hoppers. Due to fluctuations of the wall friction, shock waves are created and arches are formed, slowing down the material which follows. In regions of anisotropic stress, the rotational degree of freedom is frustrated parallel to strong stresses, so that ordering akin to anti-ferromagnetic spin coupling may be observed.

Pouring two different materials on a flat surface leads to a sandpile with stratification patterns. The mechanisms leading to this segregation of the two types are examined with experiments and numerical simulations. The stress distribution inside a sandpile depends strongly on the contact network. A relatively small polydispersity causes a reorganization of the contact network and leads to the so called stress chains, i.e. the stress at neighboring particles may vary dramatically.

Finally, the plastic shear bands occuring in large scale deformations of compactified granular media are investigated by using an explicit Lagrangian technique as well as molecular dynamics simulations with non-spherical particles.

Contents

1 Introduction

Many rather astonishing phenomena are known to occur when granular materials like sand or powders move, see Hansen and Bideau (1992), Jaeger and Nagel (1992), Jaeger et al. (1996b,a), Campbell (1990), Thornton (1993), Mehta (1994), Wolf and Grassberger (1997), Behringer and Jenkins (1997), and Herrmann et al. (1998). One example is the so-called "Brazil nut" segregation under vertical vibration, i.e. large particles rise to the top of a vibrated container that is filled with smaller grains, as examined by Williams (1976), Rosato et al. (1986, 1987), Devillard (1990), Duran et al. (1993), Knight et al. (1993), Duran et al. (1994), Dippel and Luding (1995), and Gallas et al. (1996). Other interesting phenomena are heap formation under vibration, see Faraday (1831), Walker (1982), Dinkelacker et al. (1987), Evesque and Rajchenbach (1989), Laroche et al. (1989), Rajchenbach (1991), Clément et al. (1992), Chen (1995), density waves emitted from outlets, see Baxter et al. (1989), and uncorrelated noise in the power spectra of local forces, see Liu and Nagel (1992), Baxter et al. (1993). All these effects originate in the ability of granular materials to form a hybrid state between a fluid and a solid: When the density exceeds a certain value, i.e. the critical dilatancy threshold, it resists shear like a solid. Below this density it will "fluidify", see Reynolds (1885), Bashir and Goddard (1991).

Particularly suited to study this fluidization is an experiment where sand is put on a loud-speaker or in a box on a vibrating table, see Evesque and Rajchenbach (1989), Clément and Rajchenbach (1991), Clément et al. (1992), Zik et al. (1992), Rosato and Lan (1993), Clément et al. (1993), Luding et al. (1994a), Warr et al. (1995), and Warr and Hansen (1996). Under gravity the sand jumps up and down and although kinetic energy is strongly dissipated, energy input through the boundaries is sufficient to reduce the density, thus allowing the material to flow ("fluidization"). Under certain circumstances, directed flow between top and bottom can occur in form of convection cells as has been observed experimentally when inhomogeneities in the amplitude of the vibration occur, see Rátkai (1976). More striking is that sand spontaneously can form heaps, see Evesque and Rajchenbach (1989), Clément et al. (1992), as first described already by Faraday (1831). Also within these heaps convection occurs which is one possible motor for the heap formation: Inside the heap the sand rises, pops out at the top and then slides down on the surface. The other heap-forming instability is caused by the interstitial gas and is important for sufficiently small grains. Usually those heaps have complicated shapes that change in time, and sometimes one also observes ripples and other regular structures on their surface and in the interior, see Pak and Behringer (1993, 1994), Pak et al. (1995). In very wide, rather shallow systems, the spontaneous formation of surface waves

is reported, see Douady et al. (1989), Melo et al. (1994, 1995), Metcalf et al. (1997), Shattuck et al. (1997), Luding et al. (1996a), Shinbrot (1997), Wassgren et al. (1997), even in the absence of an interstitial gas. These subharmonic instabilities may spread over the whole system and form regular structures, or, may be localized and form the so called "oscillon", see Umbanhowar et al. (1996). When particles of different sizes but equal density are put on a vibrating plate the larger particles tend to rise and after some time one observes a segregation into regions with larger and regions with smaller particles. The motor for segregation is still under discussion. However, convection seemingly enhances segregation dramatically so that other types of segregation are suppressed, see Knight et al. (1993), Duran et al. (1994), Luding et al. (1996c). When the vibration of the plate also has a horizontal component the material will flow in one direction, a technique often used for powder transport, see Pöschel and Rosenkranz (1997).

Granular media at large densities have a broad spectrum of striking effects. A packing of sand behaves like a solid when pushed, but offers no resistance to a pulling force. The famous Reynolds experiment proves that due to dilatancy a deformed elastic bag full of sand increases in volume when it is being deformed. Studying in more detail the propagation of sound in a granular packing shows a strong dependence of the wave velocity on pressure, see Goddard (1990), due to the complex network that transmits the stresses. Large deformations of granular media occur along shear planes due to an irreversible plastic instability, see Sornette et al. (1991).

In order to formalize and quantify the complicated rheology of granular media various attempts have been made. Continuum equations of motion and kinetic theories have been proposed by Savage (1979), Jenkins and Cowin (1979), Haff (1983), Homsy et al. (1992), Hwang and Hutter (1995), Goldshtein and Shapiro (1995), thermodynamic formulations by Jenkins and Savage (1983), Edwards and Oakeshott (1989a), Mehta and Edwards (1989), Edwards (1991), Herrmann (1993), cellular automata by Baxter and Behringer (1990, 1991), Désérable and Martinez (1993), Károly and Kertész (1994), Peng and Herrmann (1994, 1995), Peng and Ohta (1996, 1997), and a random walk approach by Caram and Hong (1991). However, only a few of these methods have so far given a satisfactory explanation of phenomena, like size segregation or density fluctuations. This is because it is very difficult to incorporate into these theories static friction, local rotations and other relevant microscopic mechanisms.

To gain a better understanding of the rheological effects in granular media it can be very helpful to perform computer simulations, see Cundall and Strack (1979), Campbell and Brennen (1985), Walton and Braun (1986), Bardet and Proubet (1991), Bardet (1994), Walton (1993b), Luding et al. (1994a), Ristow (1994), Pöschel and Buchholtz (1995a), Herrmann (1995), Wolf (1996), Potapov and Campbell (1996), Wolf (1996), Luding et al. (1996d,a), Luding (1997). For over two decades discrete methods have been used where in contrast to continuum approaches one treats the granular material as an assembly of particles interacting through their contacts only. This technique was introduced by Cundall (1974), Cundall and Strack (1979) to study the motion of rock masses. Since then it has been applied to statistical micromechanics, see Cundall and Strack (1979), Bathurst and Rothenburg (1988), constitutive behavior of granular soils, see Thornton and Randall (1988), Dobry and Ng (1989), Issa and Nelson (1989), creep of soils, see Kuhn and Mitchell (1989), analysis of rock-support interaction, see Lorig and Brady (1984), and many other applications in soil mechanics, see Grabinsky (1992), Ting et al. (1989). Such and similar techniques have also been applied to model size segregation, see Haff and Werner (1986), Pöschel and Herrmann (1995), Dippel and Luding (1995), outflow from a hopper, see Hong and McLennan (1992), Ristow (1992a,b), Ristow and Herrmann (1994), shear flow, see Campbell and Brennen (1985), Hanes and Inman (1985), Walton and Braun (1986), Campbell (1990), Thompson and Grest (1991) and flow down an inclined chute, see Hutter et al. (1986), Pöschel (1993), Walton (1993a), Pouliquen and Renaut (1995).

In section 2 we propose a thermodynamic description of granular materials as a first step. Loose granular media can in fact be described by a thermodynamic formalism, see Herrmann (1993), in which sand grains are treated in a similar way as molecules in a gas.

The following section 3 is dedicated to a brief introduction of the modeling approaches used later on. In particular we will present the "soft-particle" Molecular Dynamics (MD), textbooks are Allen and Tildesley (1987), Rapaport (1995), and also the "hard-particle" Event Driven (ED) method, see Allen and Tildesley (1987), Lubachevsky (1991), both for inelastic spherical particles with friction forces. We present systems of granular material fluidized in a vibrating box examined by Luding et al. (1994a,d), Luding (1995) in section 4 and discuss the role of surface roughness, wall properties and

dimension.

A series of experiments, see Athey et al. (1966), Cutress and Pulfer (1967), Blair-Fish and Bransby (1973), Lee et al. (1974), Schick and Verveen (1974), Drescher and de Josselin de Jong (1972), Michalowski (1984), Baxter et al. (1989), have shown strong density fluctuations when granular material flows under the action of gravity. Baxter et al. (1989) used X-ray diffraction experiments to visualize these wave-like patterns emanating from the outlet of a two dimensional wedge-shaped hopper. Similarly, rather erratic shock-like density waves have been observed in flows through pipes by Pöschel (1994), Ristow and Herrmann (1994). Another experimentally observed ubiquitous phenomenon in granular media seems to be the $1/f^\alpha$ noise behavior, see Schick and Verveen (1974), Bak et al. (1987), Peng and Herrmann (1995), Taguchi and Takayasu (1995). For avalanches moving down the slope of a sand pile theoretical considerations of self-organized criticality by Bak et al. (1987) led to the proposal that their size and life time distributions were power laws which was in fact verified experimentally on very small piles by Held et al. (1990) and, more recently, on rice piles with elongated grains by Christensen et al. (1996), Frette et al. (1996), Luding (1996). The growth of a sandpile can, however, also be modeled by neglecting multi-particle effects like avalanches as shown in section 7. A simplified one-dimensional one-particle model is already sufficient to lead to a complicated dependence of the angle of repose on the material parameters, see Grasselli and Herrmann (1997). Furthermore, stratification patterns can be observed when pouring two different species on the pile. The simple model leads to patterns similar as those observed experimentally.

In section 8 quasi-static granular assemblies are modeled by using the MD method, see Luding (1997), from section 3 The geometry of a sand pile is sufficiently inhomogeneous to allow for arching, see Edwards and Oakeshott (1989b), Wittmer et al. (1996, 1997), Luding (1997), Savage (1997), Wolf and Grassberger (1997), so that the pressure under the apex of the sandpile has a minimum rather than a maximum. Already small polydispersity can lead to stress chains with peculiar probability distributions of the forces, see Luding (1997).

In order to understand the formation of the fractal network of shear bands in a slowly deformed box, see Poliakov et al. (1994), Poliakov and Herrmann (1994), results obtained with the Fast Lagrangian Analysis of Continua (FLAC) method are presented in section 9. FLAC is an explicit Lagrangian technique that makes use of the classical non-associate Mohr-Coulomb plastic yield criterion that is traditionally used as a constitutive relation in continuum theory of dense granular materials. Finally, we summarize the presented results in section 10.

2 A thermodynamic approach to granular media

Subject to external forces, granular materials locally perform rather statistical motions due to their mutual collisions. For example, on a loudspeaker the individual grains chaotically jump up and down forming a gas-like cloud of colliding particles. For flow down an inclined chute, see Drake (1990), Pöschel (1993) one has a laminar flow with a well defined (average) velocity profile and a superimposed Brownian-like motion of the particles in all directions.

The above observations inspired several authors to use thermodynamic concepts to describe granular media. On the one hand a "granular temperature" $T_{\rm gr}$ was defined by Campbell and Brennen (1985), Thompson and Grest (1991), Hanes and Inman (1985), Ogawa (1978), Jenkins and Savage (1983), Jaeger et al. (1989), as $T_{\rm gr} \propto \langle \vec{v}^2 \rangle - \langle \vec{v} \rangle^2$, i.e. proportional to the kinetic energy surplus with respect to the global motion. The brackets $\langle ... \rangle$ denote an ensemble averaging. Strictly speaking this definition is thermodynamically justified if an equipartition theorem exists which is not the case for granular particles since they dissipate energy at collisions.

On the other hand, Edwards and Oakeshott (1989a), Edwards (1991), Mehta and Edwards (1989) put forward another idea for static packings: Based on the important observation that granular materials do not conserve energy they proposed to consider the occupied volume V to replace the internal energy in the usual thermodynamic formalism and define a temperature-like quantity $X = \partial V/\partial S$ which they called "compactivity" where S is the entropy. Although formally intact, this formalism is not easy to generalize to rapid flow like on a vibrating table or on an inclined plane, since the volume is not properly defined. While Edwards' approach seems intuitively correct for dense packings and the definition and use of $T_{\rm gr}$ appears to be reasonable in the limit of strong internal motions or weak dissipation the two definitions fail in the corresponding opposite limit.

Let us present in the following a thermodynamic approach to granular materials by Herrmann (1993), founded on similar principles as equilibrium thermodynamics and incorporating at least partly

the intuitive pictures of previous work: We shall consider subsystems sufficiently small to have no velocity or density gradients and for which the energy flux into them is such that energy dissipation is homogeneous. Energy conservation implies that $0 = \Delta E_{\rm int} + \Delta D - \Delta I$ where ΔD is the energy dissipated in a given time and ΔI is the energy that was pumped into the system during that time. In a steady state the internal energy $\Delta E_{\rm int}$ is like in traditional thermodynamics the change of the sum of kinetic and potential energy of all the degrees of freedom of the grains as elastic bodies (translation, rotation, elasticity, etc.). One can now treat the excess dissipated energy $\Delta \mathcal{D} = \Delta D - \Delta I$ in a similar way as the heat in usual thermodynamics.

One can express changes in $\mathcal{D}$ as $\delta \mathcal{D} = \wp \delta C$ where $\wp$ is an internal pressure acting at collisions. The extensive conjugate quantity C plays the role of a potential and should in fact be proportional to the volume of contact deformation. The "equilibrium" - which is in fact a steady state driven by the energy flux - can be defined as the ensemble *minimizing* C, and one can *postulate* in analogy to the second law of thermodynamics that C should decrease for any change of state at constant internal energy $E_{\rm int}$: $\Delta C \leq 0$ driven by the elastic repulsion between colliding grains.

As in usual thermodynamics one can now work in different ensembles. Naturally, one would work at fixed $\wp$ (granular ensemble) in which a granular potential G_r can be defined as $G_r = E_{\rm int} + \wp C$ and where at constant $\wp$ the equilibrium is given by the minimum of G_r. The response function κ defined as $\kappa = \frac{\partial \mathcal{D}}{\partial \wp} = \wp \frac{\partial C}{\partial \wp}$ measures how much more energy can be dissipated if $\wp$ is increased. On top of the granular ensemble one can build up the traditional body of thermodynamics as if the grains were a gas of particles interacting elastically. One can fix or free the number N of particles, define a "granular" temperature T_g and entropy S or impose to the system either an external volume V or an external pressure p. Special for granular media is that one could also impose an external shear τ or the dilatancy V_d, see Reynolds (1885), Bashir and Goddard (1991).

Considering a "state" given by the positions, orientations, linear and angular velocities of the grains as rigid bodies the entropy is well-defined as noted already by Edwards and Oakeshott (1989a), Edwards (1991), Mehta and Edwards (1989). A reasonable definition for a "granular" temperature T_g would then be: $T_g = \left(\frac{\partial G_r}{\partial S} \right)_{\wp}$ which is, in fact, similar to that defined previously by Campbell and Brennen (1985), Thompson and Grest (1991), Hanes and Inman (1985), Ogawa (1978), Jenkins and Savage (1983), Jaeger et al. (1989). Experimentally, $\wp$ and T_g are independent control parameters of the system: T_g is essentially driven by the amount ΔI of energy that is fed into the system per unit time. $\wp / T_g$ depends mainly on the density of collisions and can therefore increase by fragmenting the grains into smaller pieces.

3 Models for particle-particle interaction

In this section we will discuss several models for particle-particle interaction using different degrees of abstraction. We will start with methods that account for the excluded volume of the particles via a repulsive potential, either "hard" or "soft" and will relate both models to each other. The next step of abstraction is to neglect the detailed interaction at the contact but instead assuming molecular chaos so that the particles collide randomly. Then, we discuss the possibility to use lattice models as in fluid dynamics, neglecting also the discrete nature of the particles. Finally, we simplify even more and assume that it is possible to project a dynamic process, like the growth of a sandpile, back to one-particle trajectories.

The elementary units of granular materials are mesoscopic grains consisting of many atoms each ($10^{15} - 10^{25}$). When these objects interact (collide) the attractive potentials of the individual atoms can often be neglected. It is important that on a microscopic scale the surface of the grains is rough. Solid friction is the consequence: When two grains touch and their contact surface is at rest with respect to each other, a finite force F_s is needed to trigger a relative motion (*static friction*). If the contact areas slide on each other, a finite force F_d is needed to maintain the motion (*dynamic friction*). The forces follow the relation $F_d < F_s$ and depend on the normal force and neither on the velocity nor on the area of contact (*Coulomb's law*). This picture is idealized and an entire discipline called tribology, has evolved to study solid friction in depth, see Johnson (1989).

Friction has the crucial consequence that the system does *not* conserve energy on the level of the grains. Other sources of dissipation can be viscous damping or plastic deformations of the grains. Since dissipation may occur due to various reasons, we discuss in the following only simple dissipation

laws, assuming that the detailed knowledge of the interaction potential is of minor importance. In fact, more complicated laws increase the number of parameters without giving qualitatively different answers.

The difference between the two most frequently used methods is the interaction potential. For the molecular dynamics method soft particles with a power law interaction potential are assumed, whereas for the event driven method rigid particles are used. The consequence is that the duration of the contact of two particles is finite for MD but vanishes for ED.

3.1 The event driven, rigid particle method

The description of the collisions of rigid particles is based on the work of Mindlin (1949), Mindlin and Deresiewicz (1953), Maw et al. (1976, 1981). Therefore, we apply the simplified collision model introduced by Walton and Braun (1986) and recently established experimentally by Foerster et al. (1994) and Labous et al. (1997).

For given velocities before contact, three coefficients are needed to evaluate the velocities after collision. The first, the coefficient of normal restitution, r, defines the incomplete restitution of the normal component of the relative velocity. The second, the coefficient of friction, μ, relates the tangential force to the normal force, i.e. Coulomb's law. The third, the coefficient of maximum tangential restitution, β_0, delimits the restitution of tangential velocity of the contact point, to ensure energy conservation. Note that this model implies that two grains at contact either slide following Coulomb's law or stick together, see Foerster et al. (1994), Walton and Braun (1986). In the following, we apply the basic conservation laws and determine the equations for the velocities after collision.

Consider two particles with diameter d_1 and d_2 and masses m_1 and m_2. The normal unit vector for their contact is $\vec{n} = \vec{r}_1 - \vec{r}_2 / |\vec{r}_1 - \vec{r}_2|$, where $\vec{r}_i$ is the vector to the center of particle i ($i = 1, 2$). For the interaction of particle $i = 1$ with a fixed wall, we set $m_2 = \infty$, $d_2 = 0$ and $\vec{n}$ is in this case the unit-vector perpendicular to the wall-surface pointing from the contact point with the wall to the center of the particle. The relative velocity of the contact points is $\vec{v}_c = \vec{v}_1 - \vec{v}_2 - \left(\frac{d_1}{2}\vec{\omega}_1 + \frac{d_2}{2}\vec{\omega}_2\right) \times \vec{n}$, with $\vec{v}_i$ and $\vec{\omega}_i$ being the linear and angular velocities of particle i just before collision. From the momentum-conservation laws for linear and angular momentum there follows

$$\vec{v}_1' = \vec{v}_1 + \Delta\vec{P}/m_1, \tag{1}$$

$$\vec{\omega}_1' = \vec{\omega}_1 - \frac{d_1}{(2I_1)}\vec{n} \times \Delta\vec{P}, \tag{2}$$

$$\vec{v}_2' = \vec{v}_2 - \Delta\vec{P}/m_2, \tag{3}$$

$$\vec{\omega}_2' = \vec{\omega}_2 - \frac{d_2}{(2I_2)}\vec{n} \times \Delta\vec{P}, \tag{4}$$

where $\vec{v}_i'$ and $\vec{\omega}_i'$ are the unknown velocities of particle i after collision. I_i is the moment of inertia about the center of particle i and $\Delta\vec{P}$ is the change of linear momentum of particle 1 and is a function of r, μ, and β_0:

$$\Delta\vec{P} = -m_{12}(1+r)\vec{v}_c^{(n)} - \frac{2}{7}m_{12}(1+\beta)\vec{v}_c^{(t)}, \tag{5}$$

with the reduced mass $m_{12} = m_1 m_2/(m_1 + m_2)$. (n) and (t) indicate the normal and the tangential component of $\vec{v}_c$ respectively and the factor $2/7$ in the tangential part of (5) stems from the fact that solid spheres are used. r is the (constant) coefficient of normal restitution and $\beta = \min[\beta_0, \beta_1]$ is the coefficient of tangential restitution. The latter is simplified in so far that exclusively sliding or sticking is allowed. A sliding, Coulomb-type interaction has $\beta = \beta_1$, i.e. $\Delta P^{(t)}$ is limited by $\mu_w \Delta P^{(n)}$, and a sticking contact has a constant maximum tangential restitution $\beta = \beta_0 \leq 1$ due to the elasticity of the material. Using the basic conservation laws one can calculate $\beta_1 = -1 - \mu(1+r)\cot(\gamma)(1+1/q_i)$ with the collision angle γ, and the factor $q_i = 4I_i/(m_i d_i^2)$ that accounts for the mass distribution inside the particles, see Foerster et al. (1994), Luding (1995, 1998). As illustration, a schematic picture of two colliding particles is given in Fig. 1. The angular velocities are $\omega_1 = \omega_2 = 0$ immediately before collision (a) and non-zero after collision (b). For a detailed discussion of the above equations see Luding (1995, 1998).

For the simulation of rigid particles, we use an event driven method such that the particles undergo an undisturbed motion in the gravitational field until an event occurs. An event is either the

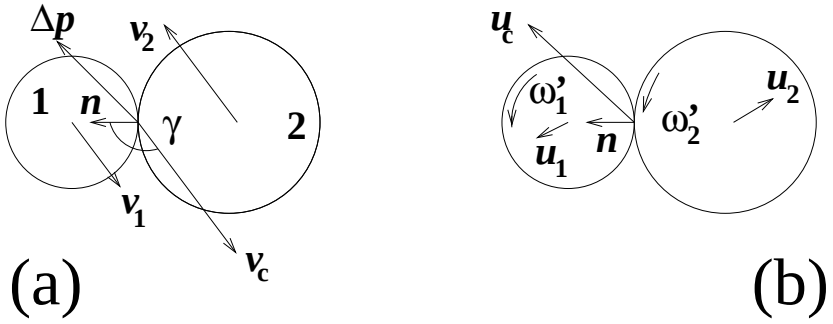

Figure 1: Typical velocities of two particles immediately before (a) and after (b) collision.

collision of two particles or the collision of one particle with a wall. From the velocities just before contact, the particle velocities after a contact are computed following (1)-(4). An efficient scalar ED algorithm was introduced by Lubachevsky (1991) which updates only those particles involved in the previous collision. Like Luding (1995), Luding et al. (1994d) we implement the algorithm of lubachevsky91 with some changes and extensions. Despite the gravitational acceleration, all contact times of particles with each other or with the lateral walls can be calculated analytically. The coefficient of normal restitution depends on the partner of the colliding particle; for example, we use r, or r_w to indicate particle-particle, or particle-wall collisions respectively. For more details on the collision model see Walton and Braun (1986), Foerster et al. (1994), Luding (1995, 1998).

3.2 The connection between soft- and hard-sphere models

In the ED method, the time during which two particles are in contact is implicitly zero. The consequence is that exclusively pair contacts occur so that the momentum change, $\Delta\vec{P}$ in (1)-(4) suffices to describe the collision completely. ED algorithms with constant r run into difficulties when the time between events, $t_{\rm ev}$, becomes too small. In systems with strong dissipation $t_{\rm ev}$ may even vanish and the so-called 'inelastic collapse' may occur, see Luding et al. (1994a), Bernu and Mazighi (1990), McNamara and Young (1992, 1993).

In MD simulations, on the other hand, $t_c > 0$ and the sum of all forces $\vec{f}(t)$, acting on a particle at time $t \in [t_0,\ t_1]$, is needed to calculate the momentum change of this particle:

$$\Delta\vec{P} = \int_{t_0}^{t_1} \vec{f}(t)dt. \tag{6}$$

In general, the contact begins at time t_0 and ends at time t_1. For a constant force $\vec{f}$ or an infinitesimally small time interval $t_1 - t_0$, the momentum change ΔP in (1)-(4) can be replaced by the term $f(t)dt$ to arrive at a differential formulation for the change of velocities $\vec{v}' - \vec{v}$ and $\vec{\omega}' - \vec{\omega}$. The primed and unprimed quantities are the values at time t_1 and t_0, respectively. For a detailed discussion of the connection between soft- and hard-sphere modelling see Luding (1998).

3.3 The Molecular Dynamics Technique

Since the modeling of realistic deformations of the particles would be much too complicated, let us assume that the overlap of two particles is the quantity important for the interaction potential. The interaction is short range, i.e. the particles interact only when they are in contact so that their penetration depth $\delta = \frac{1}{2}(d_1 + d_2) - (\vec{r}_1 - \vec{r}_2)\cdot\vec{n}$ is positive.

The first force, acting on particle 1 from 2 – accounting for the excluded volume which each particle occupies – is an elastic repulsive force

$$\vec{f}_{\rm el} = k_n\delta_0(\delta/\delta_0)^\nu\vec{n}\ , \tag{7}$$

where k_n is the elastic modulus and δ_0 is a normalization constant dependent on the non-linearity ν and the dimension. In the simplest case of a linear spring that follows Hooke's law one has $\nu = 1$.

In the case of elastic spheres in three dimensions $\nu = 3/2$, see Landau and Lifshitz (1975), i.e. Hertz contact, and for conical contacts $\nu = 2$ should be used.

The second force – accounting for dissipation in the normal direction – is a viscous damping force

$$\vec{f}_{\rm diss} = \gamma_n \dot{\delta} (\delta/\delta_0)^{\phi} \vec{n} \ , \tag{8}$$

where γ_n is a phenomenological normal viscous dissipation coefficient and $\dot{\delta} = -\vec{v}_{12} \cdot \vec{n} = -(\vec{v}_1 - \vec{v}_2) \cdot \vec{n}$ the relative velocity in the normal direction.

The simple linear spring-dashpot model (with $\nu = 1$ and $\phi = 0$) can be solved analytically and leads to a contact duration $t_c = \pi/\omega$ and a restitution coefficient $r = \exp(-\pi\eta/\omega)$, with $\omega = \sqrt{\omega_0^2 - \eta^2}$, $\omega_0^2 = k_n/m_{12}$, $\eta = \gamma_n/(2m_{12})$, and $m_{12} = m_1 m_2/(m_1 + m_2)$, see Luding (1998).

The third force – accounting for friction – acts in the tangential direction and can be chosen in the simplest case as

$$\vec{f}_{\rm shear} = -\gamma_t \dot{\xi} \vec{t} \ , \tag{9}$$

where γ_t is the viscous damping coefficient in tangential direction and $\dot{\xi} = \vec{v}_{12} \cdot \vec{t}$ is the tangential component of the relative velocity, with $\vec{t} = \vec{v}_{12}/|\vec{v}_{12}|$. Eq. (9) is a rather simplistic description of shear friction. For many applications (arching, heap formation) it is, however, important to include real static friction, see Lee and Herrmann (1993), Wolf and Grassberger (1997), which can be done by a 'static' friction force, see Cundall and Strack (1979), Schäfer et al. (1996): When two particles start to touch each other, one puts a "virtual" spring between the contact points of the two particles, and $\vec{\xi}(t) = \int_{t_0}^{t_1} \vec{v}_{12} dt$ is the *total* tangential displacement of this spring during the contact. The restoring frictional force is thus $-k_t \vec{\xi}$ (static friction). According to Coulomb's criterion, the maximum value of the restoring force is then proportional to the normal force f_n^c at this contact, with the friction coefficient μ. Cast into a formula this gives a friction force

$$\vec{f}_{\rm friction} = -\frac{\vec{\xi}}{|\vec{\xi}|} \min(k_t |\vec{\xi}|, \mu f_n^c) \ . \tag{10}$$

We note that the tangntial spring has to be kept at a maximum length $\xi_{\rm max} = \mu f_n^c / k_t$ in order to lead to reasonable agreement with contact dynamics simulations or theoretical calculations by Radjai et al. (1997). Only when particles are no longer in contact with each other the spring is removed. Main source of static friction in real systems is the geometrical roughness of the surfaces, see Pöschel and Buchholtz (1993), Walton and Braun (1993), Walton (1994), Pöschel and Buchholtz (1995b), and the same effects of particle stopping can be obtained also without Eq. (10) by using particles of complicated shapes, like crosses or polygons, see Buchholtz and Pöschel (1994), Buchholtz et al. (1995), Kohring et al. (1995), Matuttis and Luding (1997). In fact, when particles deviate from the spherical shape rotations are suppressed in dense packings under strong load. However, in some cases it is sufficient to use a combination of Eqs. (9) and (10):

$$\vec{f}_{\rm dyn} = -\min(\gamma_t \dot{\xi}, \mu f_n^c) \vec{t} \ , \tag{11}$$

a rather bold alternative to the more realistic static friction law in Eq. (10), but reasonable for many, especially dynamic situations, see Radjai et al. (1997).

3.4 The stochastic DSMC simulation method

Direct simulation Monte Carlo (DSMC) is a method first proposed by Bird for the modelling of rarefied gas flows by Bird (1994); it was also used for liquid-solid flow simulations (see Tanaka et al. (1996) and references therein). One of the advantages of the algorithm is its suitability for parallelization. Here we introduce dissipation and an excluded volume correction and apply the method to dry granular media.

In DSMC the evolution of the system is integrated in time steps τ. At each time step every particle is first moved without interaction with other particles. The particles are then sorted into spatial cells with length L and volume $V_c = L^D$, where D is the dimension. L is set to one half of the mean free path but not less than two bead diameters. The time step τ is chosen sufficiently small to assure that even the fastest particle needs several time steps to cross a cell. Between particles in the same cell stochastic collisions are assumed to take place. The rules for these collisions are taken from kinetic theory. Let N_c be the number of particles in the cell, $v_{\rm max}$ an upper bound for the relative

velocity between the particles and σ the scattering cross section of spheres ($\sigma_{2D} = 4R$, $\sigma_{3D} = 4\pi R^2$). Then

$$M_c = \frac{N_c(N_c-1)\sigma v_{\max}\tau}{2V_c} \tag{12}$$

is the maximum number of pair collisions in each cell. To obtain $v_{\max}$ we sample the velocity distribution from time to time and set $v_{\max}$ to twice the maximum particle velocity found. In order to obtain the correct number of collisions with regard to the actual relative velocities an acceptance-rejection method is applied: For a pair of particles i and j the collision is performed if

$$\frac{|\vec{v}_i - \vec{v}_j|}{v_{\max}} < Z, \tag{13}$$

where Z is a random number uniformly distributed in the interval $[0,1]$. This method leads to a collision probability proportional to the relative velocity of the particles.

Since the collision takes place regardless of the position of the particles within the cell, an impact parameter b must be chosen so that the post-collision velocities can be calculated. Molecular chaos is assumed here, b is drawn from an uniform distribution in the interval $[-2R, 2R]$ in 2D or in a circle with radius $2R$ in 3D. We tested the validity of this assumption with ED and found no deviations in the parameter range discussed below. The remainder of the collision scheme is identical with the event driven procedure, so that the normal component of the post collision velocity is $\vec{u}^{(n)} = -r\vec{v}^{(n)}$, whereas the tangential component remains unchanged.

To achieve better results at higher densities the DSMC method was extended in two respects; we refer to the modified method as DSMC2. Firstly, an offset of $2R$ was added to the particle distance along the direction of momentum transfer by Alexander et al. (1995). Secondly, we correct M_c in (12) by replacing the volume V_c of a cell with the effective free volume $V_c - V_0$, where V_0 is the volume the particles in that cell would need in a random close packing [packing fraction 0.82 in 2D, see Gervois and Bideau (1992), and 0.64 in 3D, see Jaeger and Nagel (1992)]. In a direct comparison with ED simulations, the DSMC method was applied to vibrated granular media by Müller et al. (1997) and for freely cooling granular media in the absence of gravity by Luding et al. (1998).

3.5 Lattice models

It seems natural to describe the flow of granular media by means of concepts of fluid mechanics. Taking into account the dissipation rate in the energy balance equations Goldhirsch and Zanetti (1993), Savage (1992) predicted the existence of an associated instability: Slightly denser regions have more dissipation and therefore lower pressure which, in return, generates a flow that will enhance the density. So, dissipation is responsible for the formation of clusters of high density, see Goldhirsch and Zanetti (1993). It has also been possible to derive from this kinetic gas theory, see Savage (1992), Haff (1983), Jenkins (1985), that the viscosity increases very sharply with density.

Alternatives to the direct solution of the equations of motion of fluids are the so called Lattice Gas (LG) and Lattice Boltzmann Models (LBM). These models are defined on a lattice with velocity vectors that can only point into a few discrete directions, and all have the same length. For the LBM this simplification is somewhat compensated by the fact that on each site one has more real degrees of freedom (six on a triangular lattice) than in the classical numerical techniques allowing for the definition of a local shear or a local rotation. For a more detailed description of Lattice- and Lattice-Boltzmann models, used for the modelling of granular media, see Flekkoy and Herrmann (1993), Peng and Herrmann (1994), Herrmann (1995), Vollmar and Herrmann (1995), Alonso and Herrmann (1996). Here, we will only discuss a recently proposed one-particle model, for heap formation, see Alonso et al. (1997). One-particle model means in this context that only one particle is inserted into the system and then moved by following the rules described below, until it comes to a halt. Once stopped the particle will never move again, and the next particle is inserted.

3.6 A simple one-particle lattice model

Two essential features of granular materials are (i) excluded volume, and (ii) dissipation. On a lattice, the excluded volume can be modelled by allowing no more than just one particle per site. If a particle encounters an empty site below it, it falls due to the action of gravity. If it hits the surface $h(x)$ of the granular material, there are two possibilities, either the particle stops, thus increasing the local

height of the surface by Δh, or it moves along the slope. In the traditional model by Bak et al. (1987) the decision for either of the two options depends only on the local slope. The new model also monitors the actual energy of the particle and accounts for the dissipation at each contact with the coefficient of energy restitution r^e. The energy after each contact $e' = r^e e$ is a function of the energy e before collision. Note that the restitution coefficient r and the coefficient of energy restitution are connected via the relation $r^e = r^2$. The particle will stop immediately if $e' \leq e_t$, and it will continue to jump if $e' > e_t$. Friction, and also the macroscopic surface roughness of the material, are combined in the parameter e_t, the trapping probability. If the energy is sufficiently large, the particle jumps a distance Δx that is, in the simplest case, exactly one lattice site a. In order to account for inertial effects, the model can be generalized, so that

$$\Delta x = \mathtt{int}\left[\frac{e'}{e_t}\right], \tag{14}$$

where int[] selects the integer part of the argument. Another variation of the model delimits Δx, because a particle with large e and thus large Δx will destroy the surface at each impact and thus loose more energy due to internal rearrangements in the pile. The upper bound of Δx is denoted by $\Delta x_{\max}$. In section 7 we will compare experiments and the different variations of the model, when two species of particles with different properties are poured from a point-source onto a sandpile.

4 Simulating vibrated granular media

Due to the complex dynamics and the dissipative nature of granular systems, analytical approaches, i.e. kinetic theories by Savage (1979), Haff (1983), Jenkins and Savage (1983), Campbell (1990), Hwang and Hutter (1995), are quite difficult to handle and can be solved only in small ranges of parameter space. Mazighi et al. (1994) solved the dissipative Boltzmann equation, for a one-dimensional (1D) system under vibration, in the limits of weak and strong dissipation. Furthermore, the experimental assessment of local quantities, like granular temperature or pressure, is extremely difficult. However, an experimental setup was developed that uses digital high-speed photography to track the linear and angular motion of the particles in 2D systems, see Warr et al. (1995, 1994), Foerster et al. (1994). In addition to experiments and theories, numerical simulations are an adequate tool to study the behavior of dissipative granulates and thus complement experiments and theories. The majority of the simulations on vibrated systems of granular media are performed by using the soft particle molecular dynamics (MD) method, see Taguchi (1992), Gallas et al. (1992b), Luding et al. (1994b,c), Walton and Braun (1986), Kohring (1994), but also the hard particle event driven (ED) algorithm, see Luding et al. (1994a,d), Mazighi et al. (1994), Allen and Tildesley (1987), McNamara and Young (1996), Du et al. (1995), is used. For a critical comparison of both methods see Allen and Tildesley (1987), Luding et al. (1994d,c), Luding (1994), Rapaport (1995).

We present simulations for systems of spheres with rough surfaces in two-dimensional (2D) vibrating boxes using the collision model introduced in section 3. The systems are examined by systematic variation of the parameters, as for example the coefficient of friction, μ. We find that the behavior of the system depends on the frictional properties of both, particles and walls. Introducing particle-particle friction changes the behavior quantitatively. Rough, dissipative walls lead to a qualitative change of the behavior of the system when density is low. If dissipation is not too strong and enough energy is fed into the system, e.g. via vibration of the container, the surface of the material may fluidize, see Clément et al. (1993), Luding et al. (1994a), and the energy will scale with the typical velocity of vibration rather than with the typical acceleration, see Luding et al. (1994a), Brennen et al. (1993), Rosato and Lan (1993). Simulations in 1D by Clément et al. (1993), Luding et al. (1994a), Mazighi et al. (1994) were complemented by two dimensional simulations by Luding et al. (1994a), Luding (1995) and experiments by Brennen et al. (1993), Warr et al. (1995). The potential energy E - in 2D experiments and simulations - scales with the typical velocity V to a power $\theta < 2$, i.e. $E \propto V^{\vartheta}$, in contrast to theoretical predictions by Warr et al. (1995), Lee and Dufty (1996).

4.1 System and boundary conditions

Our system is a rectangular container of width L, and open at the top. The vertical position of the bottom of the box at time t is given by

$$z_0(t) = A_0 \sin(2\pi f t), \tag{15}$$

where f is the frequency and A_0 the amplitude. The typical velocity of the motion is $V = A_0\omega$, with $\omega = 2\pi f$. The container is filled with N spherical particles with diameter d_i ($i = 1, ..., N$). If not explicitly mentioned, d_i is uniformly distributed in the interval $d_0 - w_0 \le d_i \le d_0 + w_0$, where $d_0 = 1$ mm and $w_0 = 0.1$ mm. The properties of these particles are defined through the coefficient of normal restitution r, the coefficient of friction μ and the coefficient of maximum tangential restitution β_0. As a simplification, we assume for most simulations that the bottom of the container is elastic and perfectly smooth, i.e. $r_b = 1$ and $\mu_b = 0$.

In the following, three different average quantities of the system are calculated, (i) the reduced height of the center of mass H, (ii) the kinetic energy K and, (iii) the rotational energy R. The averages are performed at phase zero, i.e. when the bottom moves upwards with velocity $V = A_0\omega$. We calculate the reduced height of the center of mass, $H = h_{\rm c.m.} - h_{\rm c.m.0}$, with the height of the center of mass, $h_{\rm c.m.} = (1/M)\sum_{i=1}^{N} m_i z_i$, the total mass $M = \sum_{i=1}^{N} m_i$ of all particles with mass m_i, and the vertical coordinate z_i of particle i. The average mass of one particle is $m = M/N$, and the height of the center of mass at rest is, see Luding (1995),

$$h_{\rm c.m.0} \approx \frac{n_b d_0}{2N}\left[(1-\sqrt{3}/2)n_h + \sqrt{3}/2 n_h^2\right] + \frac{n_o d_0}{2N}\left[1+\sqrt{3}n_h\right] \ . \tag{16}$$

Here n_b is the average number of beads per layer in the presence of walls, $n_h = {\rm int}[N/n_b]$ is the number of full layers and $n_o = N - n_h n_b$ is the number of beads in the uppermost layer. Note, that (16) is exact only for monodisperse particles. As an example, for $N = 50$, and $L = 10d_0$ we approximate $n_b \approx 9$, since due to the size fluctuations of the particles, almost always nine particles per layer are found not 10, as would ideally fit into the box. Thus we use for $N = 50$ and $L/d_0 = 10$ the values $n_b = 9$, $n_h = 5$ and $n_o = 5$, which leads to $h_{\rm c.m.0} = 2.492 \times 10^{-3}$ m. Varying n_b by ± 1 we show that H is almost independent of the specific value of n_b for velocities $V > 0.1$ m s^{-1}, as should be. For larger amplitudes or smaller frequencies as used in this study, additional tests have to be performed, in order to verify Eq. (16) for particles of different sizes.

The average potential energy per particle is mgH, with $g = 9.81$ m s^{-2} being the gravitational acceleration. Apart from the constant prefactor $m/2$, the average kinetic energy per particle is $K = (1/M)\sum_{i=1}^{N} m_i v_i^2$, with v_i being the velocity of particle i. In analogy, we define the rotational energy as $R = (q/M)\sum_{i=1}^{N} m_i(\frac{d_i}{2}\omega_i)^2$ with ω_i being the angular velocity of particle i. The prefactor q describes the mass distribution inside the particles and thus determines the moment of inertia $I = qm(d/2)^2$.

A useful concept in classical statistical mechanics of equilibrium systems is the equipartition theorem. In granular media, seen here as an example for dissipative non-equilibrium systems, energy is *not* necessarily equally distributed between the different degrees of freedom. Depending on the flow of energy, i.e. dissipation and energy-input, the boundary conditions and the collisional properties, the degrees of freedom may be activated differently, see Luding (1995), Du et al. (1995), McNamara and Luding (1998a).

In the following, density and velocity distribution functions are presented, and the partition of energy between the degrees of freedom is discussed, i.e. energy non-equipartition is observed. Simulations are compared to experiments and the influence of the wall properties on the behavior of the system is examined.

4.2 Density and velocity distribution functions

Using the direct simulation Monte Carlo (DSMC) method, the dynamics of spheres in two-dimensional vibrating boxes can be described. With an excluded volume correction for the DSMC method, as introduced in section 3, one can access even higher densities. The results obtained by DSMC are then compared with results from event driven (ED) simulations in the following.

The height of the center of mass is a measure for the energy stored in the system. To evaluate the validity of the DSMC method for this application we first compare ED, DSMC and DSMC2 in two

dimensional simulations. In Fig. 2 the height of the center of mass H is plotted against the velocity V for elastic walls and inelastic particles, while the particle number density is displayed as a function of height z for f=100Hz and V=0.11 m s^{-1}. At low excitations of the bottom plate ($V < 0.6\,\mathrm{m\,s^{-1}}$) the DSMC method becomes invalid. However, the improved DSMC2 method still gives good agreement with ED down to $V = 0.06\,\mathrm{m\,s^{-1}}$. In this case the density is about 84% of the maximum density the system has at rest. The considerably improved agreement of DSMC2 with ED can also be seen in the density profile.

In Fig. 3 the probability distribution is plotted for the horizontal (U_x) and the vertical (U_z) velocities. The agreement of DSMC2 and ED is reassuring. The mean square velocity is larger for elastic walls compared to dissipative walls and the distribution of the vertical component is asymmetric with the maximum shifted towards negative velocities. The decay for positive velocities is slower than for negative ones, due to the dissipation in the system and a net energy flux from the bottom upwards.

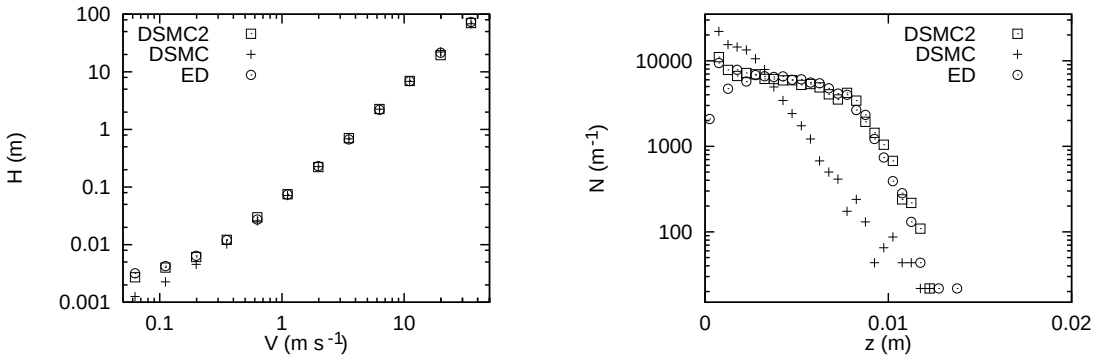

Figure 2: Comparison of the three different methods: DSMC2, DSMC and ED. Left: height of the center of mass vs. V. Right: density profile for $V = 0.11\,\mathrm{m\,s^{-1}}$.

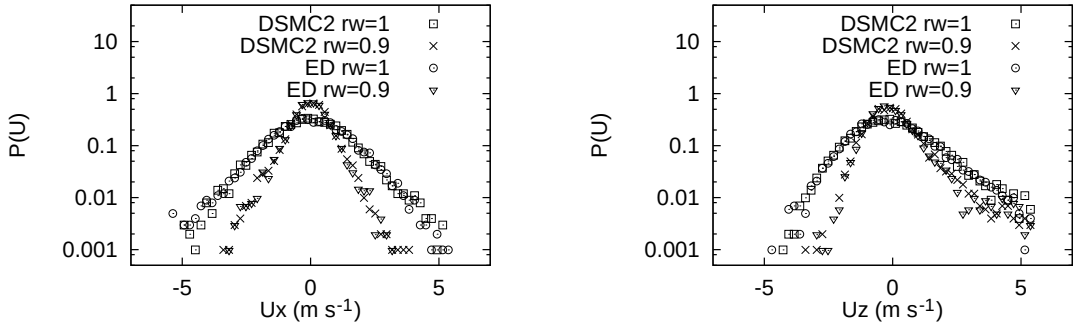

Figure 3: Semi-log plot of the probability distribution $P(U)$ of the horizontal velocity U_x (left) and vertical velocity U_z (right) for the simulation with $A = 0.00316$ m and $V = 1.98\,\mathrm{m\,s^{-1}}$.

4.3 Energy non-equipartition

At first, the behavior of the system is examined when the coefficient of friction changes. Using $N = 50$, $r = 0.9$, $\beta_0 = 0.5$, and elastic, smooth walls, we vary the coefficient of friction μ from 0 to 20. The two limits correspond to perfect sliding and to an extremely rough surface, respectively. In Fig. 4(a) the reduced height of the center of mass H is plotted against μ for two values of V, i.e. $V = 1.57$ m s^{-1} and $V = 0.314$ m s^{-1}. For $V = 0.314$ m s^{-1} the frequency f is varied, i.e. $f = 40$, 100, and 500 Hz, and for $V = 1.57$ m s^{-1} $f = 100$ Hz is used. The standard deviation of the H values lies between 10 and 15 percent of the absolute value of H. The reduced height H depends slightly on μ, i.e. for increasing μ the potential energy decreases. Note that the value of H does not change as long as V stays constant. This fact is consistent with the scaling laws found by Warr et al. (1995),

Luding et al. (1994d). Furthermore, H saturates in both limits $\mu \ll 1$ and $\mu \gg 1$. H for perfectly smooth surfaces is approximately twice as large as H for completely rough surfaces. In panel (b) the ratio $\kappa = K/R$ of the translational to the rotational energy is displayed for the same simulations as in (a). The data coincide even for different V values. The ratio K/R seems to be rather independent of the external parameters A_0 and ω. However, there exists a dependence of K/R on the coefficient of friction μ. The solid line in Fig. 4(b) is the function

$$\kappa = \frac{(2/q) + (1/\mu)}{(1+\beta_0)}, \tag{17}$$

with $q = 2/5$, and $\beta_0 = 0.5$, as derived from simulations by Luding (1995). The above κ, the effective coupling between the kinetic and the rotational energy, is obtained from the following assumptions for the limiting regimes. For weak coupling, i.e. small μ, the rotational degree of freedom is weakly excited and the behavior $\kappa \propto 1/\mu$ is expected. For strong coupling κ should not depend on μ, since the rotational degree of freedom is already maximally excited. In this regime, the translational and angular velocities are of the same order of magnitude, i.e. $v_{\mathrm{x}0}^2 \approx v_{\mathrm{z}0}^2 \approx (d\omega_{\mathrm{y}0}/2)^2 \approx v_0^2$. Here, the indices x, z, and y correspond to the directions horizontal, vertical and perpendicular to the plane of motion, respectively. Two linear and one rotational degrees of freedom are active, and with $K \approx v_{\mathrm{x}0}^2 + v_{\mathrm{z}0}^2$ and $R \approx q(\omega_{\mathrm{y}0} d/2)^2$, $\kappa \propto 2/q$ is obtained. We find that for vanishing μ or q, κ diverges. For vanishing $(1+\beta_0)$, the ratio of kinetic and rotational energy should behave like $\kappa \propto (1+\beta_0)^{-1}$, since $\beta_0 = -1$ corresponds to a smooth surface. For small $(1+\beta_0)$ almost all collisions occur in the regime of sticking contacts, for large values of $(1+\beta_0)$, only a certain fraction of the collisions is sticking, the rest are sliding contacts independent of β_0. Thus, if $(1+\beta_0)$ is small, it strongly affects the rotational velocities after contact. If $(1+\beta_0)$ is large, the effect is, however, rather weak. Therefore, the multiplicative factor $(1+\beta_0)^{-1}$ in Eq. (17) is explicitly set in evidence. In Fig. 4(c) we plot the ratio of K and H, i.e. K/H, against μ for the same simulations, as presented in Fig. 4(a). Equipartition of potential and kinetic energy, i.e. $mgH = (m/2)K$, here corresponds to a ratio $K/H = 2g$. The ratio of kinetic and potential energy is smaller than expected, except for the low frequency data (crosses). Also, except for low frequencies, the ratio K/H decreases slightly with increasing μ. In panel (d) the kinetic energy is plotted against μ; it collapses for large μ, but shows a behavior different from the scaling that was found for the potential energy in panel (a) for small μ.

4.4 Comparison with experiments

We now perform a direct comparison of our simulations with recent experiments by Warr et al. (1995). In order to reproduce the experimental setup the system width is set to $L = 165$ mm, the vibration frequency to $f = 50$ Hz, and the amplitudes are $A_0 = 0.5$, 1.12, 1.84, and 2.12 mm. For each amplitude simulations with different particle numbers $N = 27$, 40, 60, and 90 are performed. All particles have the same diameter, i.e. $d_0 = 5$ mm and $w_0 = 0$, with the coefficients of normal restitution, $r = r_w = r_b = 0.92$. The coefficients of friction are $\mu = \mu_w = \mu_b = 0.22$, and the coefficients of maximum tangential resitution are here set to $\beta_0 = \beta_{0\mathrm{w}} = \beta_{0\mathrm{b}} = 0$.

Similar to Figs. 15 and 16 in Warr et al. (1995), we plot $H = h_{\mathrm{c.m.}} - h_{\mathrm{c.m.}0}$ as a function of $V = A_0\omega$ in Fig. 5(a) and as a function of the inverse number of layers, $h = n_b/N$ in Fig. 5(b). The simulations (open symbols) are not in perfect agreement with the experimental data (solid symbols). To compare the simulations with the experiments, we perform power law fits of the form

$$H \propto V^{\vartheta} \tag{18}$$

and display the results in Table 1. Fig. 5(b) shows that also the dependence of H on the number of particles N is different in simulations and experiments. The powers χ obtained from fits to the form

$$H \propto (n_b/N)^{\chi} \tag{19}$$

are displayed in Table 2 for $f = 50$ Hz and different amplitudes. These simulations were performed with a container of infinite height; simulations in a container with height 285 mm, as in experiments, lead to the averaged powers $\overline{\vartheta} = 1.52$ and $\overline{\chi} = 0.70$, still sytematically larger than measured experimentally. The reduction of the slopes comes mainly from simulations with large amplitude and small numbers of particles in which sometimes a particle hits the top.

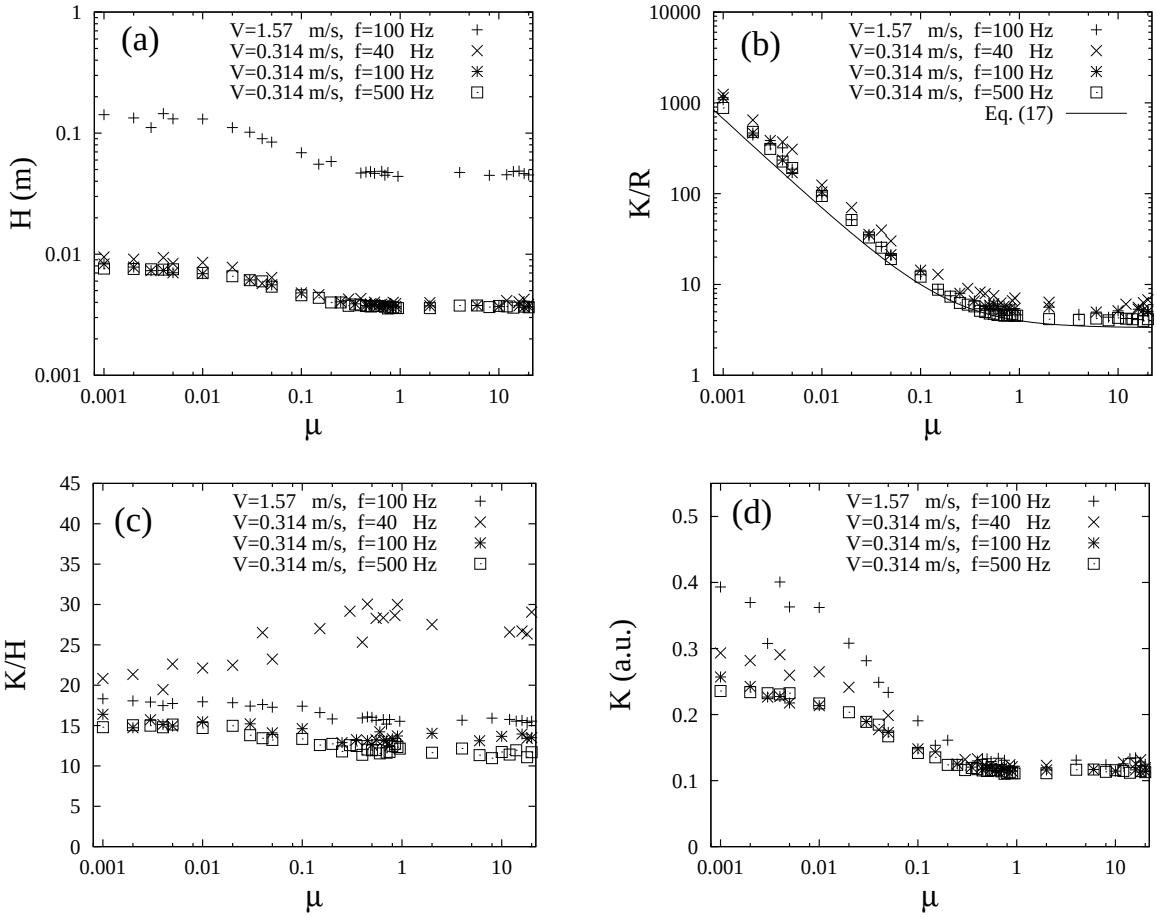

Figure 4: (a) Reduced height of the center of mass, H, plotted against μ in log-log scale. The parameters are $N = 50$, $n_b = 10$, $r = 0.9$, and $\beta_0 = 0.5$. The values of the typical velocity, V, and of the frequency, f, are defined in each figure. (b) The ratio of kinetic and rotational energy, K/R, plotted against μ in log-log scale. Simulations are the same as in (a) and the solid line represents Eq. (17). (c) Ratio of the kinetic energy and the reduced height, K/H, plotted against μ in semi-log scale. (d) Kinetic energy K, in arbitrary units, plotted against μ in semi-log scale. The simulations are the same as in (a).

One reason for such large values of the exponents ϑ and χ could be the value of r_b. Therefore, we perform the same simulations as for Fig. 5, but now using different values for the restitution with the bottom, i.e. $r_b = 0.84$ and 0.96. For decreasing r_b, we observe a decreasing H, but we do not observe a significant dependence of ϑ on r_b, and also χ decreases only slightly with decreasing r_b. Another possible reason for the discrepancy between experiment and simulation is the experimental setup which is not really two-dimensional, i.e. particles may collide with the front and back walls. We expect that in the third dimension, front and rear walls also affect the behavior of the system. Warr et al. (1995) estimated this energy loss and found that (due to wall friction between two particle-particle contacts) it was of the order of a few percent of the energy lost per particle-particle collision. Thus, further detailed comparisons of experiment and simulations are necessary to understand the effects which cause the differences.

4.5 The role of the side walls in 2D and 3D

In order to better understand the influence of the walls, we will now examine the specific role of the side walls, an examination of the role of the front and back walls is beyond the scope of this review. The strange dependency of the potential energy on the typical velocity is most obvious in a plot of H against V for all possible combinations of r and r_w. The agreement between DSMC2

N	27	40	60	90	$\overline{\vartheta}$
experiment	1.239	1.310	1.326	1.022	1.22
simulation	1.72	1.66	1.57	1.45	1.60

Table 1: The power ϑ in the law $H \propto V^{\vartheta}$ from experiments by Warr et al. (1995), and simulations by Luding (1995).

A_0 (mm)	0.5	1.12	1.84	2.12	$\overline{\chi}$
experiment	0.140	0.172	0.396	0.350	0.26
simulation	0.60	0.71	0.81	0.91	0.76

Table 2: The power χ in the law $H \propto (n_b/N)^{\chi}$ from experiments by Warr et al. (1995), and simulations by Luding (1995).

and ED for all boundary conditions shows that the particle-particle and particle-wall interaction is correctly represented. For elastic walls and dissipative particles we find $\vartheta \approx 2$ if $V \leq 0.6\,\mathrm{m\,s^{-1}}$. For inelastic walls we observe a smaller value, $\vartheta \approx 1.5$, over two log-cycles, whereas for elastic particles and inelastic walls two different regimes are seen. In the latter case $H \sim V$ for small V and $H \sim V^2$ for large V. For $V > 5\,\mathrm{m\,s^{-1}}$ the density is sufficiently small that many collisions with the walls occur before the next particle collision takes place. Therefore, if the walls are inelastic, the horizontal velocity of a particle decays between two particle collisions. Thus the dissipation of energy per unit time through the walls decreases due to decreasing collision frequency. Particle-particle collisions are necessary to trigger dissipation, and the system behaves similarly to a system with dissipative particle collisions.

Once the agreement between ED and DSMC2 is established in 2D, we can now investigate the behavior in 3D. In order to obtain densities comparable to those in 2D the number of beads is increased by a factor of 10, because the system is 10 diameters wide and deep. We estimate the height of the center of mass at rest to $H_{3\mathrm{D}}(0) = 2.2 \times 10^{-3}\mathrm{m}$ by using an ED simulation with dissipative beads and a fixed bottom plate. Irrespective of the particular boundary condition chosen, no new qualitative aspects of the behavior of the system are found when the transition from 2D to 3D is performed. This means that, effectively the physical behavior of a 2D system is recovered, because of the equivalence of the two horizontal dimensions.

We applied the DSMC method to dry granular media simulations, accounting for dissipation and excluded volume. With the corrections described above reasonable quantitative agreement between the deterministic ED method and the partially stochastic DSMC2 algorithm is obtained. This proves that the assumptions made for DSMC are correct in the parameter range discussed here and that the behavior of the system does not depend on possible correlations between collisions. We compared results obtained for various boundary conditions and found that the system shows qualitatively the same behavior for the height of the center of mass in 2D and 3D. This proves that the scaling observed is not a 2D artefact. A still open question is the extension of DSMC to larger densities up to the stable packing density.

4.6 Discussion of the dilute case

Introducing friction between particles leads to their rotational motion. By comparing potential, kinetic, and rotational energies it is found that the potential and kinetic energies are of the same order of magnitude, almost independently of the frictional properties of the particles. Kinetic, K, and rotational, R, energy are coupled via the relative velocity of the surfaces and the effective coupling parameter that relates K and R. With increasing friction, i.e. increasing roughness of the surfaces, the ratio K/R decreases, until it saturates as a function of the structure of the particles, see Eq. (17). Rough particle surfaces lead to a systematic reduction of the potential energy of the system without changing the qualitative behavior. The reduction of the potential energy is related to the additional degree of freedom, i.e. rotation. Because of the surface roughness a certain amount of kinetic energy is stored in the rotational degree of freedom. This energy is not accessible for the linear motion in the direction opposite to the gravitational force. Thus, both kinetic and potential energy are reduced

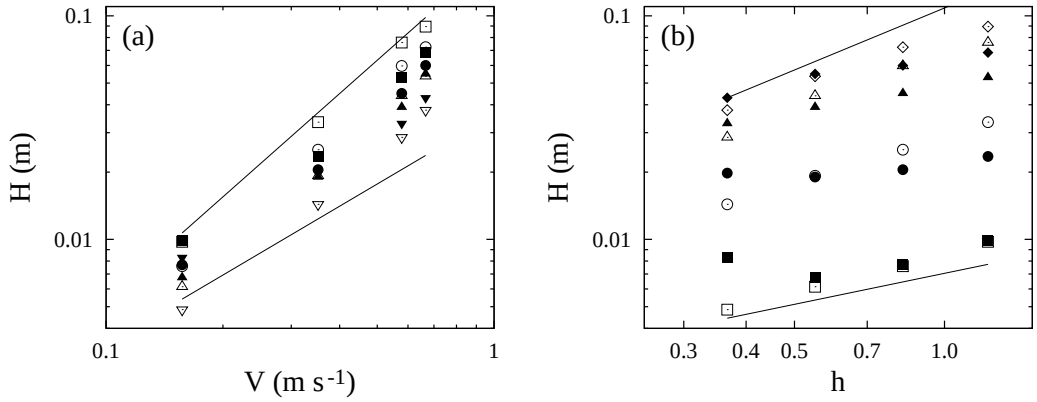

Figure 5: (a) H plotted against V in log-log scale. The parameters of dissipation are $r = r_w = r_b = 0.92$, $\mu = \mu_w = \mu_b = 0.22$, and $\beta_0 = \beta_{0w} = \beta_{0b} = 0.0$. Squares, circles, triangles and diamonds correspond to $N = 27$, 40, 60, and 90 respectively. The open symbols are simulation data, the solid symbols give the respective experimental measurements. The upper (lower) line corresponds to $\vartheta = 1.5$ ($\vartheta = 1.0$). (b) H plotted against $h = n_b/N$ in log-log scale for the same simulations as in Fig. 5(a). Squares, circles, triangles, and diamonds correspond to $A_0 = 0.5$, 1.12, 1.84, and 2.12 mm, respectively. Open and solid symbols have the same meaning as in (a). The upper (lower) line corresponds to $\chi = 1.0$ ($\chi = 0.5$).

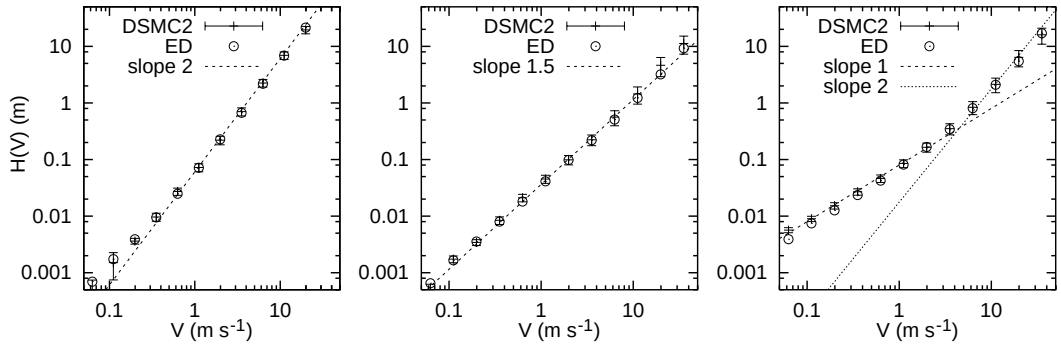

Figure 6: Reduced height $H(V) - H(0)$ with different dissipation combinations. Left: $r_w = 1, r = 0.9$, middle: $r_w = 0.9$, $r = 0.9$, right: $r_w = 0.9$, $r = 1$. The error bars indicate the standard deviation.

if rough particles are used.

Interestingly, the properties of the walls affect the system in a more complicated way. In the dilute regime smooth, elastic or smooth, dissipative walls correspond to the powers $\vartheta \approx 2$ and $\vartheta \approx 3/2$, respectively. The potential energy increases slower with V when the walls are dissipative. Collisions between particles and walls occur frequently whenever the mean free path is comparable to or larger than the system width L. Thus, the effect is stronger for less dense systems, i.e. larger H. Rough walls lead to a further reduction of the height H, because large tangential velocities relative to the walls mean strong dissipation due to friction. Overall dissipation thus depends on the frictional parameters and also on the density of the system. If one performs simulations in a container with moving, rough walls, a behavior is observed that is similar to the behavior of a system with smooth walls. Moving, rough walls lead to energy dissipation due to friction like fixed, rough walls. But sometimes, due to the velocity of the wall, energy may be fed into the system, see Luding (1995). However, a system with roughness and normal dissipation, for both particles and walls, follows the power law $E \propto V^{\vartheta}$ with $\vartheta \approx 1.33$ over two orders of magnitude in V. This result is consistent with the experimental findings of Warr et al. (1995).

Performing simulations with rotating particles, and relating the simulations to recent experiments, it was found that the height of the center of mass was of the same order of magnitude as in the experiment. Note however, that the powers ϑ and χ are systematically larger in simulations. This

suggests deficiencies with the three-dimensional nature of the experimental setup. The simulations which we compared with the experiments were performed in a small range of V and (n_b/N) values. From other simulations, see Fig. 6, the scaling law $E \propto V^{\vartheta}$ is equally obtained with a power smaller than 2. Recent theoretical approaches by Warr et al. (1995), Lee (1995) always led to the power $\vartheta = 2$. Precise comparisons of simulations, experiments, and theories are necessary to learn where the differences become significant. For ongoing research concerning dilute vibrated granular media, see Müller et al. (1997), McNamara and Luding (1998b,a), Huthmann and Zippelius (1998).

5 Simulation of size segregation

One of the most puzzling phenomena encountered in granular matter is size segregation: When a mixture of grains of the same material (equal density) but different size is shaken in a container the larger particles rise to the top. This effect has been extensively studied experimentally by Ahmad and Smalley (1973), Williams (1976), Bridgwater (1976) and has much importance in numerous industrial and geological processes, see Brown (1939). Recently, this so called "Brazil nut effect" has also attracted much interest among physicists, see Jaeger and Nagel (1992), Jaeger et al. (1996b).

Size segregation inevitably seems to contradict equilibrium statistical mechanics since the density of the overall packing increases with polydispersity and so gravity should make situations with larger particles on the bottom energetically more favourable. Rosato et al. (1987) proposed a Monte Carlo algorithm and put forward a kinetic argument to explain segregation using the fact that smaller particles are more mobile. In the same year, Haff and Werner (1986) performed Molecular Dynamics simulations of rather small systems and claimed that segregation was essentially a consequence of solid friction and the rotation of the particles. Jullien and Meakin (1992), Jullien et al. (1993) used a piling technique which is non–stochastic as compared to that of Rosato et al. (1986, 1987), Devillard (1990), Dippel and Luding (1995) and found a critical ratio $\mathcal{R}$ for the radii of spherical particles below which no segregation occurs. Based on these ideas, Duran et al. (1993) formulated a geometrical theory for segregation in which the small particles glide down along the surfaces of the larger particles. Depending on the ratio $\mathcal{R}$ of radii, the motion of the large particle takes place continuously and discontinuously. The former type of motion is found for small $\mathcal{R}$, whereas the latter type is found for large $\mathcal{R}$ above a critical dimension dependent threshold. They also presented experimental evidence for the two types of dynamics and visualized the discontinuous ascent of the larger particle through stroboscopic photos. Jullien et al. (1993) reproduced the discontinuous dynamics by including horizontal random fluctuations into their model. Dippel and Luding (1995) generalized Rosatos model by allowing for small random upward motion and reproduced the experimental findings of Duran et al. (1993), i.e. they showed that segregation takes place on an extremely slow time scale in the *absence* of convection.

Parallel to these local theories there has been the "convection connection": It is known experimentally, see Rátkai (1976), and numerically, see Taguchi (1992), Gallas et al. (1992b), that shaken assemblies of spheres form convection rolls which are attached to the walls of the container. For weak shaking the convection rolls only appear on the surface. Knight et al. (1993) and Ehrichs et al. (1995) presented experiments where segregation was due to this convection and the fact that larger particles encounter difficulties to enter again the downwards moving bulk once they are on the surface. They also verified an exponential decay of the convection strength as function of depth for weak shaking, see Knight et al. (1995). Duran et al. (1993, 1994) verified segregation due to convection in two dimensions for strong shaking and claimed that the above mentioned local mechanisms are at work at weak shaking.

Large scale Molecular Dynamics simulations show, see Pöschel and Herrmann (1995), that also for weak shaking convection can be responsible for segregation but in a more intricate way: Under certain conditions the larger particle is able to pull down the convection rolls due to the more efficient momentum transfer and then rises within the convective flow. Because of the exponential decay of convection with depth the ability to rise depends critically on the vertical position of the larger particles.

Throughout the simulation the parameters were $\nu = 1$, and $\phi = 0$ (linear spring-dashpot) $k_n = 3\times10^6\ \mathrm{g\,s^{-2}}$ (elastic modulus), $\gamma_n/m_{12} = 100\ \mathrm{Hz}$, $\gamma_t/m_{12} = 1\ \mathrm{Hz}$ (phenomenological normal and tangential friction coefficients) and $\mu = 0.5$ (Coulomb friction coefficient). We considered $N = 950$ particles with diameters uniformly distributed in the interval $d_i \in [1.7, 2.3]$ cm and with masses $m_i = \pi d_i^2 \rho/2$, with density $\rho = 1\ \mathrm{g\,cm^{-2}}$. These parameters correspond to the contact duration for

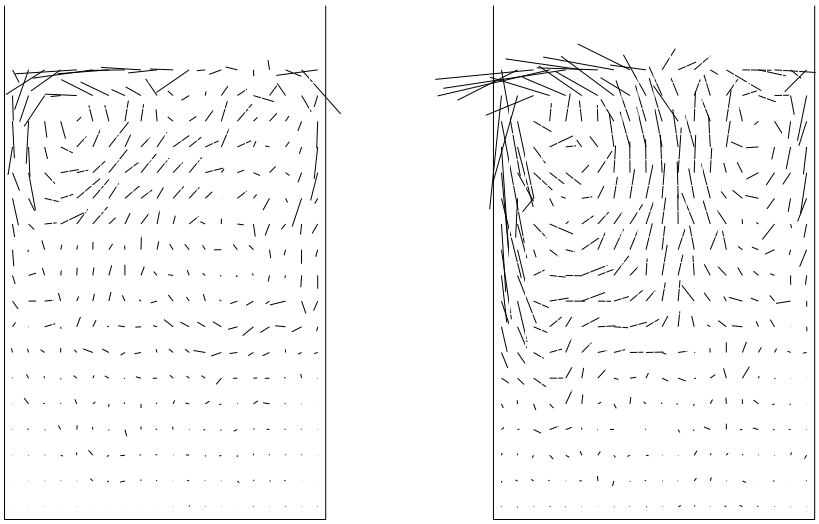

Figure 7: Convection rolls in systems without (left) and with the larger particle (right) for $f = 2.8$ Hz. The box is $L = 50$ mm wide and filled to a height of about 70 mm. The big particle with $R_1 = 4$ cm triggers convection rolls. The velocities were obtained by averaging over 50 shaking periods of the box, from Pöschel and Herrmann (1995).

small particles $t_c = 4.6 \times 10^{-3}$ s and the restitution coefficient $r \approx 0.6$. As in the previous chapter, the particles are put into a two-dimensional box with walls, here made of particles with the same material characteristics as the grains, vibrating according to Eq. (15) with $A_0 = 2$ cm. Gravity acts in negative z–direction with $g = 9.81\ \mathrm{m\,s^{-2}}$. The time step for the numerical integration of the Gear predictor–corrector scheme of fifth order was $\Delta t = 5 \times 10^{-5}$ s, well separated from the contact duration t_c by two orders of magnitude.

Segregation and convection behavior have been investigated by Pöschel and Herrmann (1995) as function of the vibration frequency f in two different systems, either all particles are small or one single big particle of radius $R_1 = 4$ cm located in the centre of the box close to the bottom is added. In order to investigate closer what happens at the onset of segregation let us keep all the other parameters fixed. Fig. 7 shows the convection cells without the larger particle (left) and with the larger particle (right) for a frequency $f = 2.8$ Hz, i.e. at the onset of segregation. The convection cells with and without the big particle, differ significantly, while they are quite similar for larger or smaller frequencies. This indicates that at the onset the presence of the big sphere triggers convection which finally leads to segregation. Indeed we find that convection is always present when segregation happens for the time-scales of a few hundred vibration cycles. Much slower segregation, taking place without convection during about many thousands of vibration cycles, as reported by Duran et al. (1993), was not investigated with the MD method. It is important to note that if one is sufficiently close to the onset of segregation by just putting the larger particles one row lower, one may entirely suppress the effect of segregation. This dependence of segregation on the height is quite strong and has so far not been discussed in the literature. By changing the frequency f very slowly and measuring the convection flow through a plane at a certain height we observed that the transition from the fluctuation regime to the convection regime is very sharp within the numerical precision ($\Delta f = 0.05$ Hz). Moreover, when increasing the frequency the transition occurs almost exactly at the same frequency as when decreasing the frequency, i.e. there is no hysteresis.

The triggering of convection cells by the big particles is investigated more quantitatively by calculating the convective flux Φ defined as the sum of material (mass) flow in the centre of the box j_{top} and the flow close to the walls j_{bot} by considering that these flows have opposite signs. The flows j_{top} and j_{bot} are defined as the sum over all particles which move in one direction minus those moving in the opposite direction. Thus, Φ corresponds to the number of particles that change from one cell to another, in a certain direction, within one vibration period. In fact, we measure for each particle whether the positions at subsequent nodes of the vibration are on different sides of a height line, where the height of the box was divided into 80 height lines between the bottom of the box and

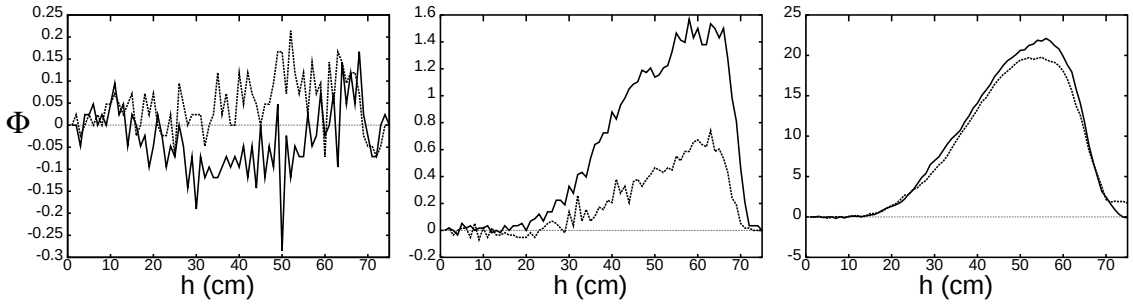

Figure 8: Strength of the convection rolls measured through the flux Φ as a function of the height h, for $f = 2.6$ Hz (left panel), $f = 2.8$ Hz (middle panel) and $f = 3$ Hz (right panel). The height h is measured such that the bottom is at the origin of the axis; note the different vertical axis scaling from Pöschel and Herrmann (1995)

the surface of the packing. Fig. 8 shows the convective flux Φ through planes at different heights h for both systems and for the different frequencies. For $f = 2.6$ Hz we find almost no directed flow but only fluctuations. For $f = 3$ Hz both systems, with and without large particle, behave similarly, as could also be observed in Fig. 7. For $f = 2.8$ Hz, however, the convection cells clearly extend deeper due to the presence of the larger particle. Apparently the larger particle is able to pull the convection cells down. In the central case, $f = 2.8$ Hz, the convection rolls are stronger and reach deeper inside the material when the big particle is present, so that this triggered convection roll catches the big particle and forces it to rise to the top.

This effect can be explained by the fact that in the region around the large particle the accelerations are higher since the momentum is transferred with less dissipative loss through the larger particle than through a corresponding pile of smaller particles of the same volume. We measured the sum of the absolute values of the forces of all the particles in a region around the position of the large particle and averaged it over time. The region was ring shaped with the inner border of radius 4.5 cm and the outer border of radius 8 cm. At the onset of segregation ($f = 2.8$ Hz) the average force of the small particles around the large particle is about 15% larger than that of the small particles in the same volume in a system containing no large particle. This effect is strongest in the lower part of the ring shaped region. For $f = 2.6$ Hz the difference is only 5%. Therefore the accelerations in the region around a large particle are larger than if no particle would be present. We believe that this increase in high frequency oscillations is responsible for pulling the convection rolls down. It is, however, interesting to note that the granular temperature (kinetic energy) in this region is roughly the same in the two systems.

One can see from Fig. 7 that the convection cells decay very sharply in strength but that even in the deep regions some essentially horizontal motion occurs. This is reminiscent of the stroboscopic pictures of Duran et al. (1993, 1994) implying that even in the low acceleration regime some particles move inward horizontally. Within our framework, however, this motion could be interpreted as the exponentially weak tail of the convection rolls. On the other hand, it may simply be a consequence of mass-conservation, i.e. the small particles fill up the volume left free by the large particle when it rises.

Next we investigated the dependence of the onset of convection on the ratio $\mathcal{R}$ of radii. Note that in our case $\mathcal{R} = R_1/(1\text{ cm})$ because the mean radius of the small particles is 1 cm. For $f = 3.2$ Hz a big particle of radius $\mathcal{R} = 4.0$ was immediately moving up. We also studied the cases $\mathcal{R} = 3.5$, $\mathcal{R} = 3.0$, $\mathcal{R} = 2.5$ and $\mathcal{R} = 2.0$, for which the large particle remains a certain time on the bottom before it suddenly rises quite rapidly. Fig. 9 shows a typical evolution of the vertical position of the big particle with $\mathcal{R} = 2$. The times before the upwards motion starts do not noticeably depend on $\mathcal{R}$ and are of the order of 30 s. Once the large particle arrives at the top it performs an oscillating motion up and down (whale effect) that was also observed experimentally by Duran et al. (1993, 1994). This motion seems to be due to the convection rolls: When $\mathcal{R}$ is small, the oscillating motion is regular because a small particle suffers less difficulty in reentering the bulk from the surface and following the convective motion. For large $\mathcal{R}$ the whale effect is less pronounced and a more erratic horizontal motion is observed. Particles with smaller $\mathcal{R}$ also seem to dip deeper into the bulk showing that the convection cells can move them more efficiently.

In conclusion, it seems that segregation of granular media in a vibrating box in two dimen-

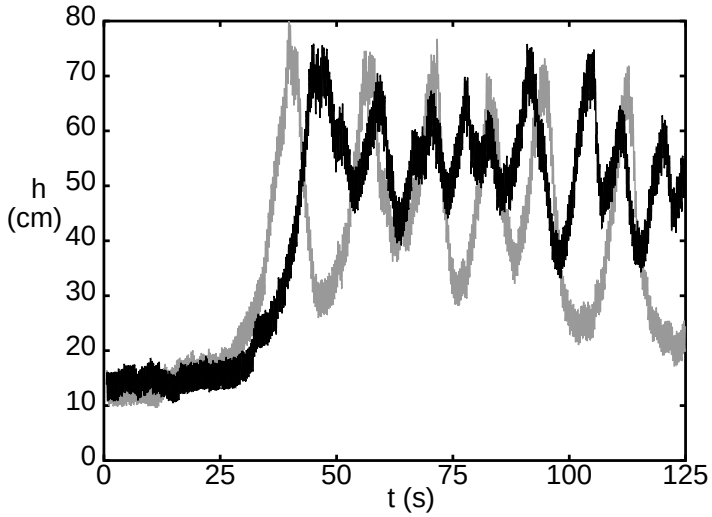

Figure 9: Evolution of the vertical position of the big particles as function of time, $\mathcal{R} = 2.0$ (grey curve) and $\mathcal{R} = 3.0$ (black curve) with $f = 3.2$ Hz, from Pöschel and Herrmann (1995).

sions is intricately connected to convection. The large particles, surrounded by a region of higher acceleration, loosen the material and thus deepen the penetration of the convection rolls from the top into the medium. After some time the larger particles are caught by the lower part of the rolls and pulled upwards. This triggering effect is only relevant close to the characteristic onset frequency of segregation which is sharply defined and strongly dependent on the initial depth of the large particle. Once the large particle is on the top it periodically moves up and down driven by the convection cells.

In addition to convection, arching and geometry are also important as pointed out by Duran et al. (1993) and Dippel and Luding (1995). How the large particles move in the exponentially weak convection field before being lifted upwards, and how the motion depends on $\mathcal{R}$ is probably best described by the local arching mechanism proposed by Duran et al. (1993, 1994). The fact that the whale effect of larger particles is less pronounced is certainly due to their lower mobility because of steric hindrance effects as formulated by Rosato et al. (1986, 1987).

Many of the details of segregation are still not completely clear, and in particular in three dimensions additional geometrical effects might play a role. This as well as other questions are difficult to study conclusively with a numerical technique due to the excessive requirements in computer time. It would for instance be interesting to see what happens when the box is so wide that the walls of the box are much farther away from the large particle than the height of the packing. In this experimentally relevant case the walls would not be able to cause or stabilize the convection rolls in the bulk. Simulations with periodic boundary conditions have, however, provided rather similar results as with fixed boundaries, see Gallas et al. (1992a). It would also be interesting to study larger ratios $\mathcal{R}$ in order to verify predictions made about characteristic values of $\mathcal{R} \approx 12$ in 2D and $\mathcal{R} \approx 3$ in 3D, see citejullien92,jullien93,duran93, but for that case one would need to consider substantially larger systems in the sense of particle number. Three dimensional calculations have been made by Gallas et al. (1996), but there the length scales are even smaller. The limitations in observation time due to the computational requirements also puts limits on the determination of the segregation velocity. We cannot exclude that particles rise on time scales much larger than those which are numerically accessible, see Dippel and Luding (1995).

6 Simulating the Flow through Hoppers and Pipes

The outflow of granular materials from hoppers and silos is an important technological problem although it seems to be so common place and standard technology. After many years of uninterrupted service a silo might one day suddenly sucumb under a "siloquake" or similar shock phenomena of surprising violence causing considerable harm. In fact silos and similar equipment are by orders of magnitude the industrial structures most susceptible to collapse. The reason for these catastrophic events is that the forces exerted by the flowing granular material against the wall of the container can fluctuate by many orders of magnitude.

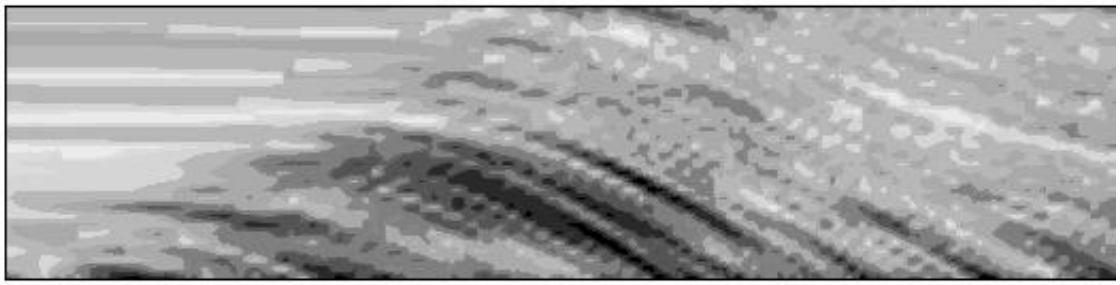

Figure 10: Spatial density fluctuations (vertical) for a typical outflow simulation, as a function of time (horizontal). For more details see Ristow and Herrmann (1994).

6.1 Fluctuations

Using similar techniques as in section 5 but including the Coulomb (dynamic) friction of Eq. (11) and rotations of particles, simulations were made for the flow out of a hopper by Ristow (1992a,b), Ristow and Herrmann (1994). For the flow through a pipe, the results from ED simulations are presented by Duran et al. (1996), Luding et al. (1996d).

From simulations of the flow out of a hopper, see Ristow (1992a,b), the existence of a minimal outlet diameter was reported, below which clogging occurs due to arching. The minimal outlet size is larger for equal sized particles than for randomly distributed radii, since the rheology is very different when particles are monodisperse: For a random distribution of radii the acceleration occurs on a ramified structure that has strong temporal fluctuations. Particles of equal size form regular, crystal-like domains and the motion occurs between the blocks. This block motion has been described in detail in the experiments by Drake (1990).

For the following simulation we use the Hertz interaction $\nu = 1.5$ with linear damping $\phi = 0$ as expressed in Eqs. (7) and (8). The elastic moduli are $k_n = 10^6\ \mathrm{g\,s^{-2}}$ and $k_t = 10^3\ \mathrm{g\,s^{-2}}$, the damping constants are $\gamma_n/m_{12} = 100$ Hz and $\gamma_t/m_{12} = 500$ Hz, and the friction coefficient is $\mu = 0.5$. The particles, each with diameter d_i drawn from a Gaussian distribution with width w around mean $d_0 = 1$ mm, are subject to the gravitational acceleration $g = 9.81\,\mathrm{m\,s^{-2}}$ and the time-step used for the simulations was $\Delta t = 2 \times 10^{-}4$ s. The silo walls are made of particles with the same material properties as the flowing grains. In Fig. 10 a space-time diagram of the density inside a silo is plotted, where space is binned in intervals of 1.56 d_0. The silo has an outlet of width $D = 10d_0$ and the walls are tilted by $\Theta = 30°$. High and low density correspond to light and dark regions respectively. When particles of equal size are used one observes equally well developed density patterns. The effect is reduced when the diameter D of the outlet becomes too large. If it is too small the flow of particles can entirely stop due to arching. The critical diameter D_0 when this arching sets in has been studied before with similar techniques, see Ristow (1992a,b).

Regions of a given density (the same grey-scale) form curved stripes: First, the particles are accelerated by the gravitational acceleration, and later the flow takes place with an almost constant speed. This agrees with the experimental findings by Baxter et al. (1989); in those experiments, density waves move downwards for rather small opening angles. We observe no structure in distance or magnitude of the waves. In order to obtain better quantitative information on the stresses in flowing granular media, we examine the outflow from a silo and focus on the stresses at the walls – a quantity that is also accessible experimentally.

When considering smooth walls, i.e. when all wall particles having the same radii, we do not find density waves and the power spectrum looks significantly different. It shows an upward curved slope with increasing frequency which one also finds when configurations block during the outflow. A similar effect was also found in simulations of flow on an inclined plane by Pöschel (1993).

In the following we use again the Hertz interaction $\nu = 1.5$ with linear damping $\phi = 0$. The elastic moduli are $k_n = 10^8\ \mathrm{g\,s^{-2}}$ and $k_t = 10^3\ \mathrm{g\,s^{-2}}$, the damping constants are $\gamma_n/m_{12} = 500$ Hz and $\gamma_t/m_{12} = 500$ Hz and the friction coefficient is $\mu = 0.5$. With these parameters we measure for typical velocities a restitution coeffcient of $r = 0.7$. The time-step used for the simulations was $\Delta t = 5 \times 10^{-6}$ s. The simulation volume is rectangular with width 10 cm and height 40 cm, as displayed in Fig. 11. The material is initially filled into the upper half, and the silo outlet is centered

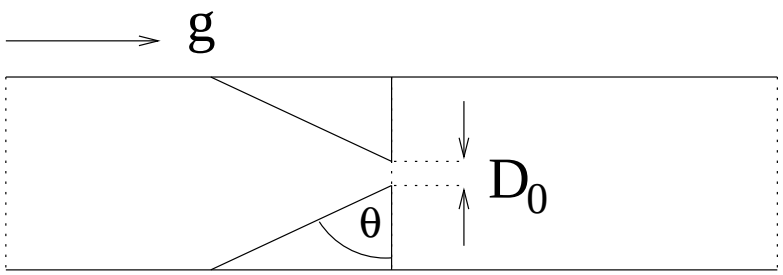

Figure 11: Schematic drawing of the silo geometry, the top is left and the bottom is right.

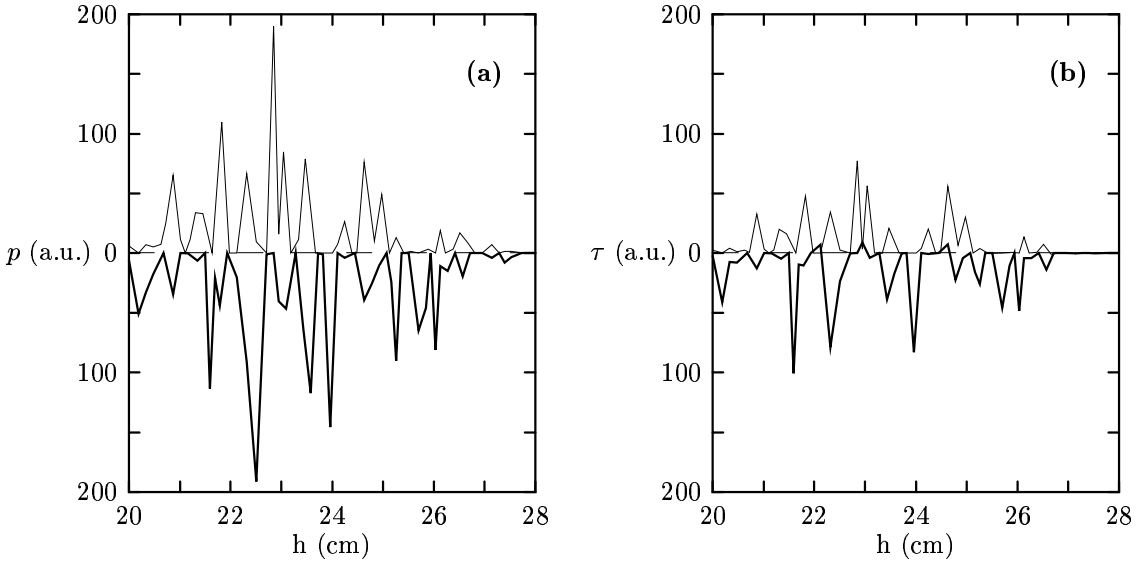

Figure 12: Distribution of (a) normal force p and (b) shear force τ at the wall of the hopper with outlet at height $h = 20$ cm. The data are taken 0.165 s after opening the outlet of a hopper with $\Theta = 40°$ and the upper and lower curves give the forces on the left and right wall respectively, from Ristow and Herrmann (1995).

at height 20 cm with width $D_0 = 2$ cm. The right (left) hopper wall is tilted counterclockwise (clockwise) by an angle Θ from the horizontal. The particles are initially randomly placed in a large volume above the outlet. After they settled due to the action of gravity, the outlet is opened and the particles start to flow. Particles are continuously added from above to guarantee steady state conditions.

In order to get quantitative information about the flow, the stress at the side walls of the hopper can be measured. From the normal (p) and the tangential (τ) components of the force acting on each of the wall-particles, averaged over 1000 time steps, the situation at time $t = 0.165$ s after the opening of the outlet is presented in Fig. 12. We observe very strong spatial fluctuations and an asymmetry of stresses, i.e. the stresses at the left and right wall (upper and lower curve respectively) are not the same at a given height. Furthermore, the shear force is at least half as big as the normal force due to the friction coefficient of $\mu = 0.5$. The curves of normal and shear stress have similar shape, meaning that frictional forces are mainly activated.

Baxter et al. (1993) also measured the stresses acting on the walls of a three dimensional hopper with an opening angle of 45° during the outflow of sand. They observed a power law decay in the spectrum of the time dependence of the normal stress (pressure) where the exponent strongly depended on the run. Measuring the fluctuations of the quantity $S = \sqrt{p^2 + \tau^2}$ which are of the same order as the mean value, one cannot deduce any apparent correlations. More quantitative information are presented in Fig. 13 where the power spectrum, $\hat{s}$, of the time sequences of S is plotted, i.e. the square of the amplitude of its Fourier transformation. For sufficiently open hoppers, like for $\Theta = 55°$,

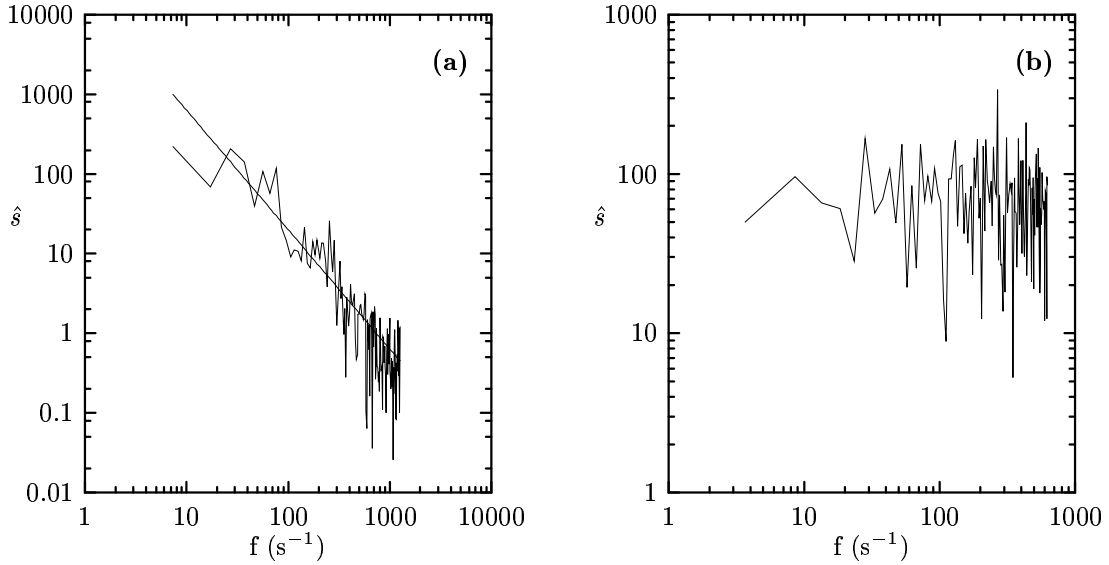

Figure 13: Log-log plot of the power spectrum $\hat{s}$ of the stresses (measured in arbitrary units) 11 particle diameters above the outlet for different angles (a) $\Theta = 40°$ and (b) $\Theta = 75°$. The straight line in (a) indicates an exponent of -1.8. The data are from Ristow and Herrmann (1995).

the spectrum decays with a power law over at least one order of magnitude with an exponent of about 1.3. This is in very good agreement with the experimental results of Baxter et al. (1993) which worked at the same opening angle. Their power law, however, extends over a much larger range than in the simulation because the computer requirements limit the observation times to several minutes while the real experiments can be carried out over many hours.

It is very interesting to note that if the hopper walls become more inclined the spectrum changes abruptly and becomes white noise. Savage (1993) found a similar situation in numerical calculations of the wall stresses in shear cells as function of density: Only at rather high densities the power spectrum showed a power law while for lower densities he observed white noise. In our case, although the density cannot be varied, a change in the opening angle determines whether there are stagnation zones or not. Evidently the density in the flowing regions is lower than in stagnations zones.

Investigating the force distribution and the shape of the stagnation zones in outflowing hoppers one observes an interesting dependence on the opening angle: In the case of funnel flow ($\Theta \approx 75°$), there are no stagnation zones, and the power spectrum of the stresses against the walls indicates white noise. By opening the angle one finds stagnation zones and a power law spectrum. This leads one to suspect that the power law in the stress spectrum does not originate from the power law in the density fluctuations, see Baxter et al. (1989), Ristow and Herrmann (1995), because the density fluctuations also follow a power spectrum in the case of funnel flow. It seems more likely that the stagnation zones act like "noise transformers" in which essentially uncorrelated random kicks emerging from the outflowing core are transmitted through the complex contact network to the wall. Similar observations have been made with the propagation of shock and sound waves in dense packed boxes by Liu and Nagel (1992).

6.2 Decompaction

Effects like recurrent clogging, see Pöschel (1994), and density waves, see Peng and Herrmann (1994), Baxter et al. (1989, 1993), Lee and Leibig (1994), are frequently observed during granulate processing. Density waves have been found in simulations to occur in a steady state regime by Peng and Herrmann (1994), Lee and Leibig (1994) or in experiments, related to gas-particle interactions (pneumatic effects) by Raafat et al. (1996, 1997). In the spirit of current efforts dealing with model granular materials by Clément et al. (1992), Knight et al. (1993), Duran et al. (1994), Warr et al. (1994) the problem of a 2D granular material made up of rather large beads is attacked. The size of the particles is large enough so that the influence of the surrounding gas can be neglected. The advantages of such

material are a direct optical observation of the particles and the possibility of tractable computer simulations.

Recent observations of approximately V-shaped *microcracks* in vertically vibrated sand-piles by Duran et al. (1994) led to the problem of gravity driven vertical motion of sandpiles in 2D containers, see Duran et al. (1996), Luding et al. (1996e,d,b). In a continuously vibrated container with rough walls, the cracks appear periodically at different positions in the pile and exist only during a short interval of time (e.g. for a few milliseconds at a vibration frequency of 15 Hz). Therefore, an experiment was designed which allows a much longer observation of the dynamics of these *microcracks*. Hence, we study the fall of a 2D granular material inside a rectangular container with frictional lateral walls. We examine the modes of decompaction, which is a basic problem related to the general dynamics of non-cohesive powders. This paper reports a series of experiments, paralleled by computer simulations based on an event-driven algorithm, including rough and rotating particles.

For the experiments, a set of monodisperse oxidized aluminum beads of diameter $d = 1.5$ mm was used by Duran et al. (1996), like in previous works on model granular materials by Clément et al. (1992), Duran et al. (1993, 1994). These metallic beads are initially arranged in an ordered triangular network inside a vertical 2D cell made up of two glass windows for visualization and two lateral vertical walls of plexiglass. The width of the cell is typically 3.6 cm and the heights of the arrays range from one diameter to 19 cm, while the gap between the glass windows is marginally greater than one diameter d. This setup minimizes friction with the front and back windows while maintaining strong friction between the pile and the lateral boundaries and thus mimics a convenient 2D granular object.

The cell containing the pile is initially closed at its lower outlet by a 1 mm deep aluminum blade which can be moved downward at an acceleration of approximately $3g$. The whole setup is carefully aligned in order to make sure that the blade does not touch the cell when moving. The downwards air drag induced by the moving blade might induce artificial effects at the beginning of the falling process. We checked this by testing that a single bead or a single layer of beads falls according to the acceleration of gravity g, so that the influence of the surrounding air will be neglected in the following. The recording setup consists of a charge-coupled-device (CCD) camera interfaced to an image processing device. The definition of the origin of time, i.e. the time when the fall starts, is measured via an additional setup which uses a He-Ne laser, the beam of which is cut-off when the blade starts moving downwards.

The observation and recording of a large number of experiments in different containers leads to the conclusion that during the fall discontinuous decompaction may occur via cracks. In Fig. 14 snapshots of a typical experiment are presented (a) complemented by the results of numerical simulations (b). For details on the simulations and the relevance of the parameters see section 3. The development of the cracks starts in the lower part of the pile and ascends progressively inside the bulk in both, experiment and simulation.

From the experimental data two very important features are discoverable which will be considered in more detail below: Almost perfectly smooth lateral walls are unlikely to induce cracks during the fall, so that the pile often remains compact. In contrast, rough walls unavoidably introduce cracks. If a crack occurs in the lower portion of the pile, it quite generally increases in size as the fall proceeds. If a crack occurs in the upper part, it tends to close and disappear during the fall. This stability can be explained with a simple generalization of Janssen's theory, see Janssen (1895), Duran et al. (1996); it leads to the conclusion that larger piles are stronger decelerated than small piles. Thus, a crack which opened in the upper half of the pile is likely to close again, because the lower portion of the pile is larger and thus stronger decelerated than the upper part.

For the numerical modeling, we are interested in the situation when a rather compact array of particles begins to fall and progressively decompacts. We use a box of width L and initially arrange N particles with diameter d on a triangular lattice with lattice constant $s = 1.01d$. Each particle is assigned a random velocity, uniformly distributed in the range $-v_0 \leq v_i(0) \leq v_0$ in both, the horizontal and vertical directions. This rather regular system is now allowed to reach a steady state, i.e. we start the simulation at $t = -t_r$, using $r = r_w = 1$ and $\mu = \mu_w = 0$. A typical average velocity in our simulations is $\overline{v} = \sqrt{< v^2 >} = 0.05$ m s^{-1} for $t = 0$. Due to the rather low kinetic energy, the array of particles is still arranged on a triangular lattice, except for a few layers at the top which are fluidized, see Fig. 14(b). In a typical simulation, we use $L = 20.2\ d$ and $N = 1562$, so that the array consists of about 80 layers. At time $t = 0$ we remove the bottom, switch on dissipation and friction and let the array decompact. We used different initial conditions, keeping all other

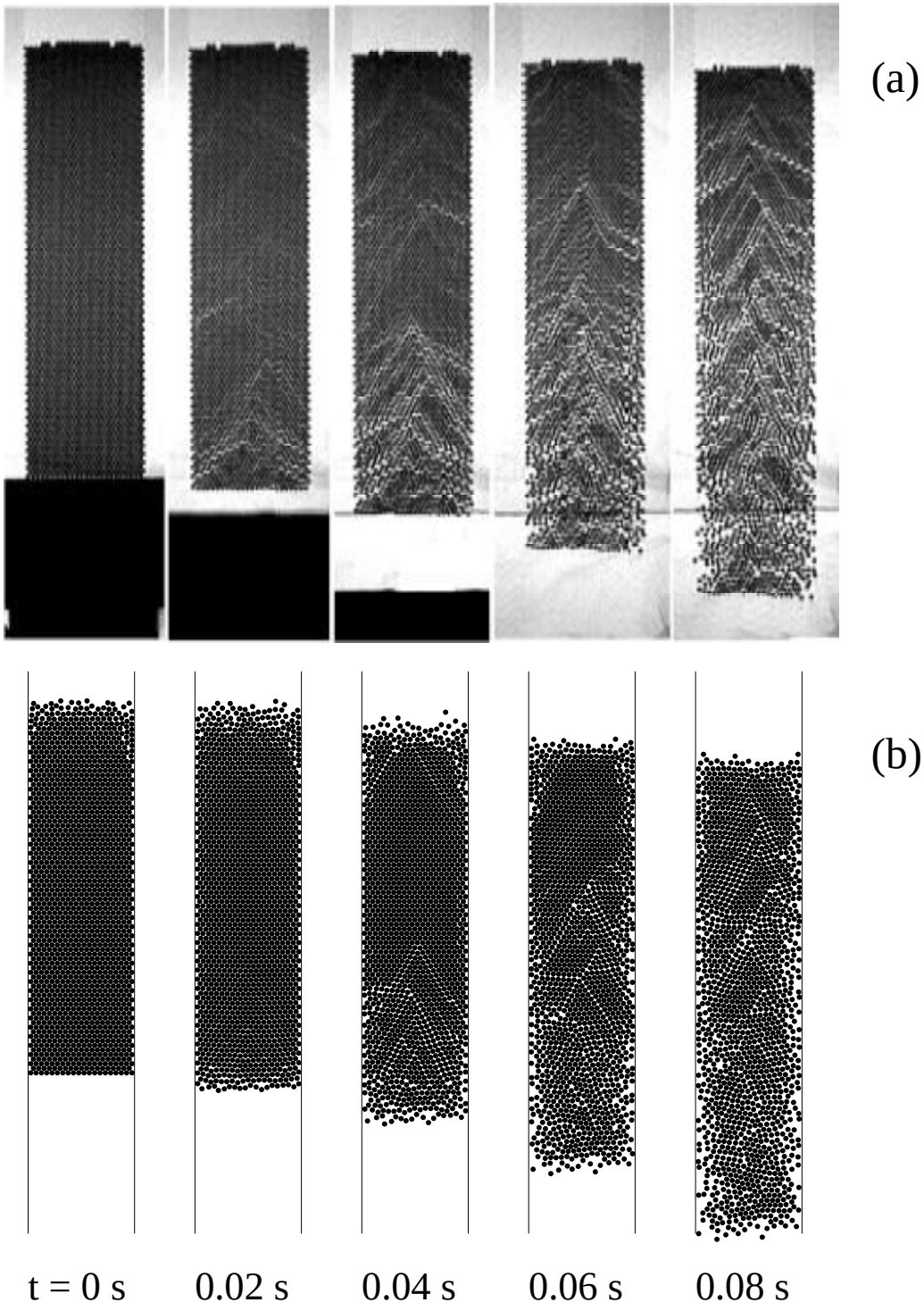

Figure 14: (a) Experiment: Successive snapshots (aperture time 1/2000 s) taken at 0.02 s intervals after the piston has been removed. We use $L = 24\ d$ and 103 layers so that $S_0 \approx 3.7$. (b) Simulation: In a container of $L = 20.2\ d$ and with 80 layers so that $S_0 \approx 3.5$; $r = 0.99$, $r_w = 0.98$, $\mu = 0.5$, $\mu_w = 1.0$, $\beta_0 = \beta_{0\mathrm{w}} = 0.2$, and $\overline{v}(t = 0) \approx 0.05\ \mathrm{m\,s^{-1}}$ was used, from Duran et al. (1996).

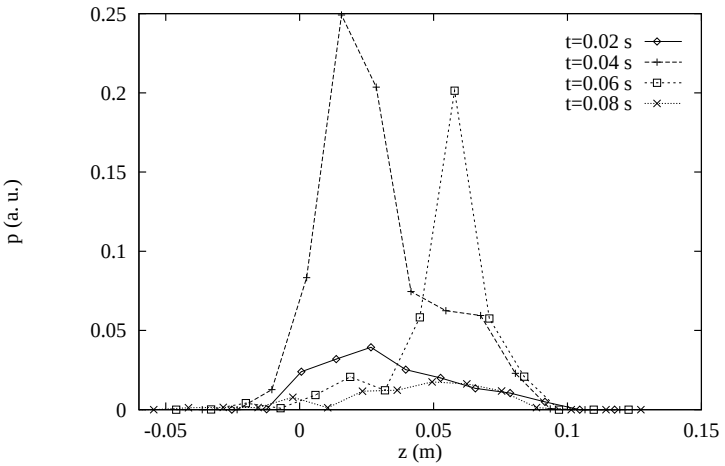

Figure 15: Plot of the pressure on the side walls as a function of height, obtained from the numerical simulations of Fig. 14(b). The integration interval is $\Delta t = 0.01$ s and each data point corresponds to a wall segment about six layers high, from Duran et al. (1996).

parameters fixed and found strong fluctuations in position and shape of the cracks. However, *the cracks are a reproducible effect*, almost independent of the initial conditions. When decreasing the tangential friction, μ_w, the cracks vanish since the pile falls with only weak perturbations from the lateral walls.

Since the comparison between experiments and simulations seems satisfactory, we investigate, via simulations, the problem of stress in the pile, see Walton and Braun (1986), Bouchaud (1994), and in particular the stresses the pile exerts on the lateral walls during the fall. From simulations, the pressure on the side walls is obtained by integrating the normal component of the momentum change, Eq. (5), of those particles which collide with the wall within the time $t - \Delta t$ and t. In Fig. 15 we chose $\Delta t = 0.01$ s and plotted the pressure as a function of height so that each data point represents the normal stress on a part of the wall about 6 layers high. For $t = 0.02$ s (diamonds) we still have a rather small pressure, whereas for $t = 0.04$ s (crosses) the pressure increases by almost one order of magnitude in the lower part of the pile. As can be imagined, this increase is strongly correlated to the occurrence of cracks. During the fall of the array arches, vaults or, in put otherwise, contact chains may be built up, corresponding in our simulations to a large number of collisions per unit time and thus to a great amount of momentum change. Such an arch can sustain particles above it, at least for a short time, and thus allow a crack to open below it. As can be seen in Fig. 15, these arches disappear after a short while and then allow the pressure to relax and the falling to proceed further. At time $t = 0.06$ s (squares) cracks are also formed in the upper part of the pile; they are again connected to strong stress. For even longer times, $t = 0.08$ s ($\times$-symbol) the particles are already too much diluted near the walls, and contact chains are no longer likely.

Before a crack can become visible, a certain time passes during which it opens. The reason for a crack to open has been identified as the fluctuations of either the wall surface, see Duran et al. (1996), or the particle motion, see Luding et al. (1996d). Thus, fluctuations lead to a momentum wave in the material. A part of the material is decelerated and the material from above hits this slower plug and causes a new, possibly stronger momentum wave. The increased pressure on the sidewalls may lead to an even stronger deceleration so that eventually a crack opens below the plug – and becomes visible only that late.

As long as the material is dense, one expects a frustration of the rotational degrees of freedom. A rotation of one particle in a triangular array is not possible if it is in contact with its six neighbors, which are also pairwise in contact. This picture is valid in case of a clockwork – however, the surfaces of granular particles are coupled via friction which permits sliding.

During simulations as presented in Fig. 14(b), the angular velocity of two neighboring particles

is random. Only when regions with strong stresses exist in the system and when this stress system is anisotropic a clear spin order can be observed. In Fig. 16 we present the spins of the particles from a simulation with $L \approx 20.2$, $H = 80$, $r = 0.96$, $r_w = 0.92$, $\mu = 0.5$, $\mu_w = 1.0$, and $\beta_0 = \beta_{0w} = 0.2$, at time $t = 0.04$ s.

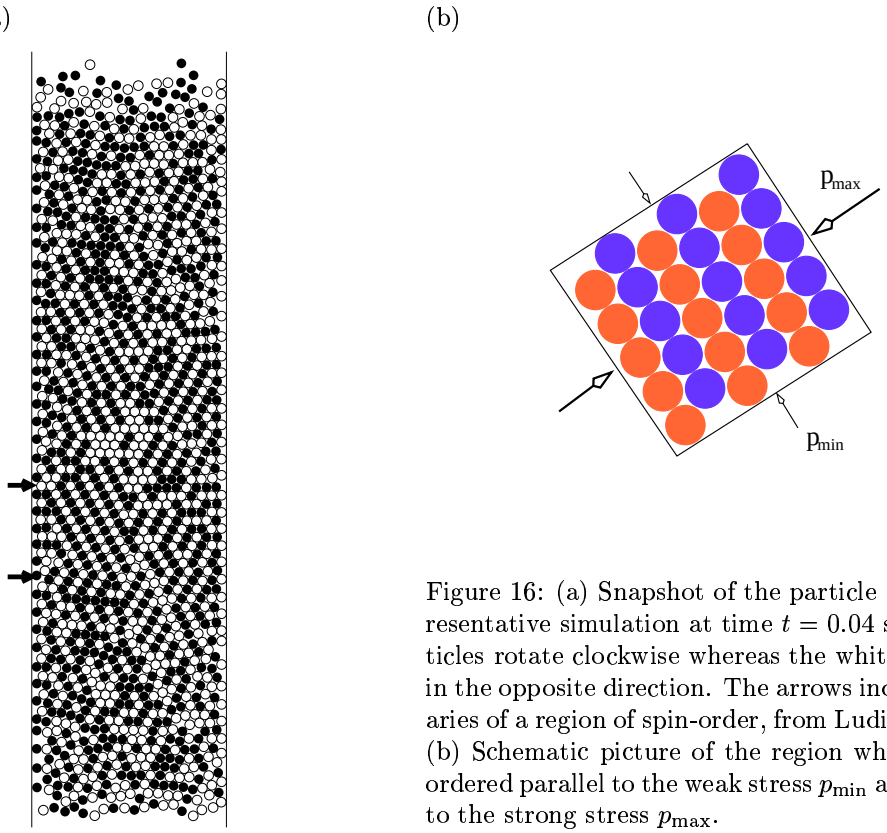

Figure 16: (a) Snapshot of the particle spins from a representative simulation at time $t = 0.04$ s. The black particles rotate clockwise whereas the white particles rotate in the opposite direction. The arrows indicate the boundaries of a region of spin-order, from Luding et al. (1996d). (b) Schematic picture of the region where the spins are ordered parallel to the weak stress $p_{\min}$ and perpendicular to the strong stress $p_{\max}$.

In the lower left half of the pipe, we observe an array of ordered spins. In Fig. 16(b) we show schematically that the spins tend to have the same direction along the line of weak pressure and have alternating direction along the direction of maximal pressure. When the stress is high, the surfaces of the particles are strongly coupled and neigbours rotate in opposite directions, i.e. the particle surfaces likely stick together and the particles roll over each other. In the minimum-pressure direction, friction is less active and sliding is possible. This picture, together with the arrangement of spins in Fig. 16(a), implies an arch-like structure within the falling pile, where strong stresses are found perpendicular to the lines of spins with equal direction.

In summary, we observe no steady regime for the falling dynamics of an initially compact granular material: the assembly decompacts progressively and accelerates downwards. Looking in more detail at the geometrical patterns formed by the grains, we observe either a *discontinuous decompaction* or a continuous one. The discontinuous decompaction is the result of cracks breaking the array into pieces from bottom to top. Both, experiments and simulations verify two basic predictions deduced from a simple continuum model by Duran et al. (1996) based on a dynamic extension of the theory by Janssen (1895). First, as long as no cracks occur, the theory predicts the acceleration of the top of the pile as a function of the aspect ratio: for increasing height, the acceleration of the top decreases. Second, if some crack occurs, it is stable only in the lower half of the pile and both blocks, hence detached, will fall with a larger acceleration and will separate further. Experiments show that cracks are rarely formed whenever the lateral walls are optimally polished; cracks always appear when the surface roughness is larger than typically 10^{-6} m. On the other hand, in simulations, the surface is perfectly flat. Nevertheless, cracks are always observed for coefficients of friction close to the experimental value, since, as mentioned above, the ED algorithm requires the use of a non-zero thermal agitation in order to provide dynamical interactions by collisions. This eventually introduces fluctuations in the system that may cause cracks, even when the coefficient of friction is constant and

the wall is flat. In order to test whether cracks are primarily induced by external fluctuations such as heterogeneities at the lateral walls, we suggest a comparison with Molecular Dynamics calculations, which do not explicitly require an internal noise. Moreover, the simulations have shown another important feature: strong pressure fluctuations are connected to the occurrence of arches and cracks and thus are propagating upwards.

As expected, the down falling motion is equivalent to the upward motion of a pile in a continuously vibrated box. Cracks, originated by the side walls, are oriented to oppose the motion of the particles relative to the lateral walls. The cracks are approximately following the geometry of the triangular network such that they occur mainly at angles of 30 degrees relative to the walls. Note that also a weak proportion of cracks with other angles is observed, see Fig. 14(b). Thinking in terms of arches or vaults anchored at the lateral walls, we note that the inverse V-shape of the contact chains is consistent with the natural shape of stable arches in a triangular network. This is reminiscent of the concept of 'free fall arches', see Brown and Richards (1970), which sustain a plug of granulate above freely falling particles. Along this line, we may tentatively extrapolate our results to 3D situations by conjecturing that a similar discontinuous decompaction process might occur via the successive formation and destruction of arches. As far as we know, the existence of cracks in monodisperse 3D as well as in polydisperse systems have not been reported so far.

7 Dynamics of sand pile growth

An experimental investigation of the size segregation induced by the flow of a binary granular mixture in a two dimensional vertical Hele Shaw cell has been performed by Grasselli and Herrmann (1998). The granular mixtures are made of equal masses of sand and glass beads, the latter having a smaller angle of repose and a smoother surface. Depending on the size ratio (rough / smooth) of the particles of the two species, we have shown that three different situations of segregation can be obtained. First, a perfect segregation between the two media with a sharp interface is found for a ratio lower than approximately 0.8, a continuous segregation with no interface occurs for a ratio close to unity and finally, stratification which consists in the formation of alternating layers of each medium arises for a size ratio greater than 1.5. We studied precisely this last case and reported that the absolute size of particles, the cell wall separation and the mass flux of the mixture can strongly modify the stratification process. In that case, the most significant information (the layer wavelength) is drastically changed. Also new experiments were started on the tail and on the slope of a heap constructed between two vertical walls, see Grasselli and Herrmann (1997). The particles are injected in the cell from the left. The right wall induces a boundary condition similar to that in silos. Preliminar results show that the slope of the heap strongly depends on the distance between the left and right walls and also on the initial energy of the particles poured in the cell. We are currently investigating the form of the tail to find its mathematical formulation, see Alonso and Herrmann (1996), Herrmann et al. (1998).

The purpose of this project is to determine the macroscopic angle of repose from the microscopic characteristics of the particles, see Alonso et al. (1997). We simulate the development of a pile of granular matter on a two-dimensional lattice. Our model includes the effects of friction, dissipation of energy by the particle-particle collisions, and sticking of the particles to the pile. The model depends only on a few parameters, so that a large number of particles (more than 10^6) may be simulated. In these simulations, we obtain that due to the discretization, the angle of repose of the pile behaves as a complete *devil's staircase* when varying the model parameters. Such fractal devil's staircases have the peculiar property that the function varies only on a set of zero measure.

Additionally, using a mixture of two different granulates with different physical properties, we have been able to observe stratification patterns (Fig. 17) which are similar to those experimentally observed and reported in the literature. Specifically, we examined the segregation which occurs if a mixture of different particles is poured on a pile. The aim of this work is to find a model which can describe all the stratification patterns which are known to occur in real sandpiles.

Using the discrete one-particle numerical model described in section 3.5, we were able to find different types of stratification depending on the maximum jump width allowed. The first version of the model allows exclusively jumps from one lattice site to the next. The result of the corresponding simulation is presented in Fig. 17(b). The stripes are rather thin and are varying in length. A modification of the model accounts for the inertia of the particles so that particles with high energy

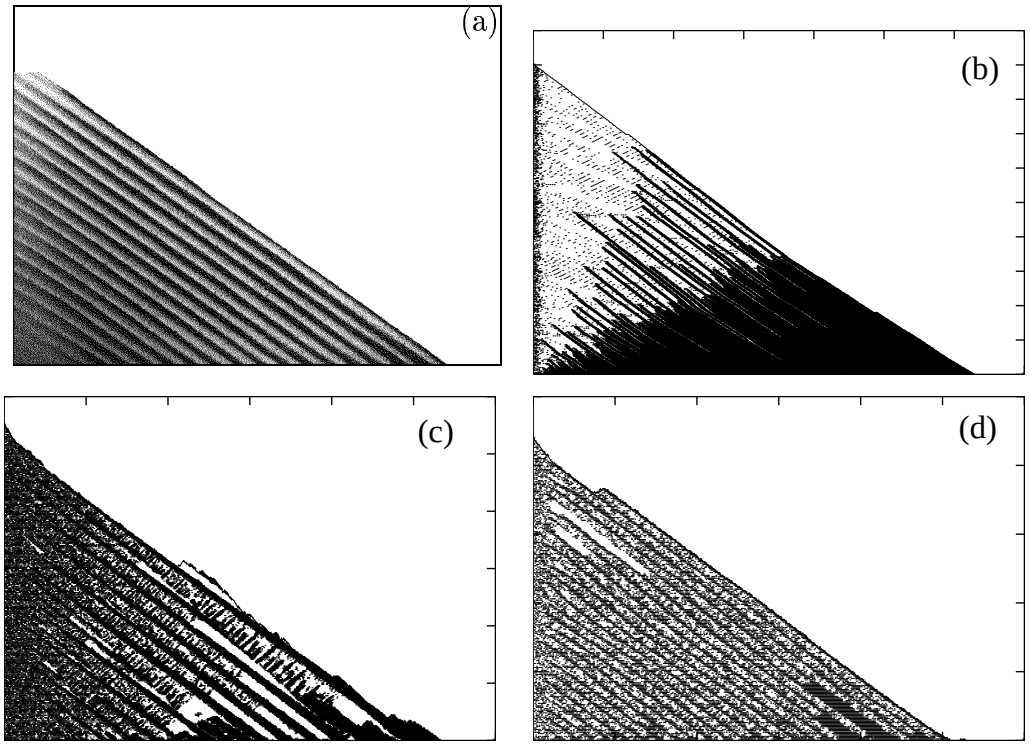

Figure 17: (a) Experimental picture of granular stratification obtained by pouring a binary mixture between two vertical walls. Stratification-patterns generated by the one-particle model ($e_{t1} = e_{t2} = 1$, random initial energy $0 \leq e_{01}, e_{02} \leq 2$, and $N = 135000$) with (b) constant jump width ($\Delta x = a$, $r_1^e = 0.8$, $r_2^e = 0.740$), (c) with energy dependent, unlimited jump width ($r_1^e = 0.8$, $r_2^e = 0.794$), and (d) limited jump width ($\Delta x_{\max} = 4a$, $r_1^e = 0.8$, $r_2^e = 0.760$). The model is described in section 3.5.

also perform longer jumps. The simulation in Fig. 17(c) leads to much thicker strata but as difference to the experiments the strata seem to grow with the system size. The last variation allows for inertia up to a certain maximum jump-width $\Delta x_{\max}$ that determines the width of the stripes in Fig. 17(d). The limitation of the jump-width can be argued to be necessary, since particles impacting on the surface with high energy will loose much more energy since many other particles may move and also dissipate energy.

A more refined model that considers four different values of r^e and e_t for each possible pair of interacting partners, see Makse and Herrmann (1998), leads to stripes in better agreement with those observed in experiments, see Fig. 17(a).

8 Quasi-static granular assemblies

In contrast to the dynamic simulations of sandpile growth, silo- or pipe-flow, and size-segregation in vibrated containers, we focus in the following on quasi-static situations. We are interested in the stress distribution inside a sandpile made of the simplest possible imaginable model material. This is a piling of almost identical spherical particles in 2D. Tangential forces like friction are neglected, see Luding (1997), Luding and Matuttis (1997), Matuttis and Luding (1997).

8.1 Stress distribution

One of the many interesting features of granulates is the stress distribution in static or quasi-static arrays. In contrast to a liquid, the pressure in a silo, filled with e.g. grains, is not increasing linearly with depth, but saturates at a certain value, see Janssen (1895). This is due to internal friction and due to arching, so that the walls of the silo carry a part of the weight of the material. In sandpiles no walls are present so that the situation may be different, i.e. the total weight of the pile has to be

carried by the bottom. However, the distribution of forces below and also inside the pile is not yet completely understood. Experiments on rather large piles often show that the normal force has a relative minimum below the top of the pile, the so-called dip, see Trollope and Burman (1980), Smid and Novosad (1981). On a much smaller scale, the stress chains are observed, i.e. stresses are mainly transported along selected paths and the probability distribution of stress spans orders of magnitude, see Liu et al. (1995), Radjai et al. (1996), Ouaguenouni and Roux (1997).

One simple model pile is an array of rigid spheres, arranged on a diamond lattice, i.e. with four nearest neighbors each, see Liffman et al. (1992), Hong (1993). The force beneath such a pile is constant in contrast to the experimental observations, and also periodic vacancies in such a configuration do not lead to a dip in the pressure at the bottom, see Huntley (1993). The variation of the size of some of the particles or an attractive force between the particles may lead to a non-constant force below the pile, see Liffman et al. (1994). Continuum approaches by Edwards and Oakeshott (1989b), Bouchaud et al. (1995), Edwards and Mounfield (1996), Wittmer et al. (1997, 1996) may lead to a dip in the vertical stress if the appropriate assumptions for the constitutive equations are chosen. Edwards and Oakeshott (1989b) introduced the notion that a pressure minimum can result from compressive stresses aligning in fixed directions. Wittmer et al. (1997) and Wittmer et al. (1996) concretized this idea recently with calculations in agreement with the experimental data by Smid and Novosad (1981). A lattice model based on a random opening of contacts, used by Hemmingsson et al. (1997), also shows the dip in average over many realizations. Different numerical simulations show a dip in the absence of friction for specific boundary conditions, see Luding (1997), or when sufficiently polydisperse particles are used, see Matuttis (1998). The non-linearity of the law for the forces and the shape of the frictionless particles seem to have a minor influence, see Luding and Matuttis (1997), Matuttis and Luding (1997), whereas the history of the formation of the pile is crucial for the stress distribution, see Matuttis (1998). Paralleling the simulations by Luding (1997), an analytical, exact solution was presented by Oron and Herrmann (1997). For more information on related research see a review by Savage (1997), and the publications by Savage, by Cantelaube & Goddard, and by Bouchaud, Cates, & Claudin in the book by Herrmann et al. (1998).

Here, we focus on properties of granular systems in the absence of friction. By neglecting solid friction, we will examine to what extent phenomena like stress chains and arching depend on friction. However, we are confronted here with what could be called "geometrical friction", as the particles restrict the motion of their neighbors due to excluded volume effects; this makes it possible to create a stable pile, see Luding (1997), Oron and Herrmann (1997). Without contact friction, energy may still be dissipated by e.g. viscous deformations, modelled here by a simple viscous dashpot, active during the contact. Since we are interested in static arrangements of particles in the gravitational field, we use strong viscous damping, in order to reach the steady state quickly. For the relaxation of the array we use a molecular dynamics (MD) procedure, see Cundall and Strack (1979), Allen and Tildesley (1987), as described in section 3, in order to allow contacts to open and to close. The MD method is not the best choice for a fast relaxation, but closing and opening contacts is implemented straightforwardly.

In the simulations N spherical particles with diameters d_i ($i = 1,...,N$) are used. If not explicitly mentioned monodisperse spheres of diameter $d_i = d_0 = 1.5$ mm are employed. The N particles are placed into a container with different boundary conditions at the bottom and also different system sizes. Starting from a regular closely packed triangular arrangement with L particles in the lowermost layer $M = 0$ at the bottom, we model heaps of slope 60^o or 30^o by forming layer M with $L_M = L - M$ and $L_M = L - 3M$ particles, respectively, as displayed in Fig. 18. The number of particles is thus $N^{(60)} = H^{(60)}(L+1)/2$ or $N^{(30)} = H^{(30)}(L - 3(H^{(30)} - 1)/2)$ with the number of layers $H^{(60)} = L$ or $H^{(30)} = \text{int}[(L-1)/3] + 1$. The largest simulated pile has $L = 100$ and thus $N^{(30)} = 1717$ particles.

The initial velocities and overlaps of the particles are set to zero, gravity is slowly tuned from zero to the selected magnitude and the system is simulated until the kinetic energy is several orders of magnutide smaller than the potential energy, and the stresses no longer vary with time. The particles at the bottom layer $M = 0$ are either fixed, or may slide horizontally and penetrate the bottom vertically. When sliding is imposed, only the outermost particles are horizontally fixed by the sidewalls.

An important quantity that allows insight into the state of the system is the stress tensor σ, see Goddard (1986), Bathurst and Rothenburg (1988); in the static case it is defined as

$$\sigma_{\alpha\beta}^{(i)} = (1/V^{(i)}) \Sigma \; q_\alpha f_\beta, \tag{20}$$

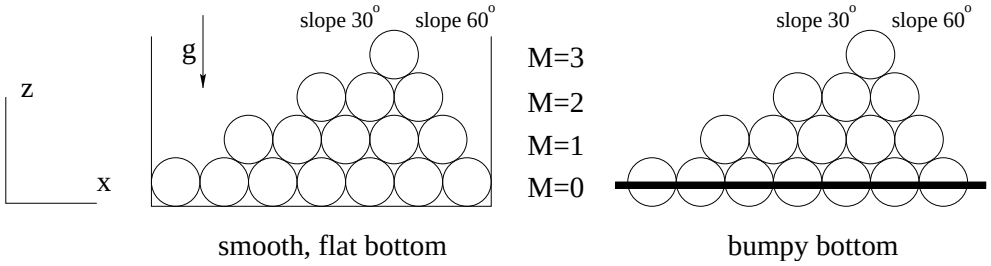

Figure 18: Schematic drawing of a pile in a box with smooth, flat bottom (left), and on a bumpy bottom (right), with $L_0 = 7$. The solid bar at the right indicates that the particles in row $M = 0$ are fixed, so that the first relevant row with mobile particles is $M = 1$ with here $L_1 = 5$.

where the indices α and β indicate the coordinates, i.e. x and z in 2D. This stress tensor is an average over all contacts of the particles within volume $V^{(i)}$, with q denoting the distance between the center of the particle and the contact point, and f denoting the force acting at the contact point. Throughout this study we average over the contacts of one particle (i) to obtain the stresses for one realization.

From a static configuration of "soft" particles we may now calculate the components of the stress tensor $\sigma_{xx}, \sigma_{zz}, \sigma_{xz}$, and σ_{zx} and also define $\sigma^+ = (\sigma_{xx} + \sigma_{zz})/2$, $\sigma^- = (\sigma_{xx} - \sigma_{zz})/2$, and $\sigma^* = \sigma_{xz}$. Since tangential forces are neglected, the particles are torque-free and we observe only symmetric stress tensors, i.e. $\sigma_{zx} = \sigma_{xz}$. The eigenvalues of σ are thus $\sigma_{\max,\min} = \sigma^+ \pm \sqrt{(\sigma^-)^2 + (\sigma^*)^2}$, and the major eigenvalue is tilted by an angle

$$\phi = \arctan\left(\frac{\sigma_{\max} - \sigma_{xx}}{\sigma_{xz}}\right) = \frac{\pi}{2} + \frac{1}{2}\arctan\left(\frac{2\sigma_{xz}}{\sigma_{xx} - \sigma_{zz}}\right) \tag{21}$$

from the horizontal in the counterclockwise direction.

In the following, the horizontal coordinate x is scaled by the width l of the pile, i.e. $X = x/l$, and $X = 0$ corresponds to the lower left end of the pile. In order to find the correct scaling for the stress we assume following Liffman et al. (1992, 1994), as a simplified example, a rigid triangle with the density ρ, the width l, the height h, and the mass $m = \rho hl/2$. Since the material is rigid, we find a constant force at the supporting surface, so that the pressure is also constant $p = mg/l = \rho gh/2$. Thus we will scale the stress by the pressure p and further on use the dimensionless stress tensor

$$S = \frac{2\sigma}{\rho gh} = \frac{\sigma l}{mg} = \frac{\sigma 2a}{hmg}, \tag{22}$$

with the volume $a = hl/2$ of the triangular pile. Apart from the components of S we will also plot the stress tensor in its principal axis representation, i.e. for each particle we plot the scaled major principal axis along ϕ and the minor axis in the perpendicular direction.

8.2 Variation of the Width of the System

In this subsection we will examine the difference between the theoretical predictions for the stresses and the numerical simulations, see Liffman et al. (1994), for a 30^o pile. The theory is based on the assumption that the contact network is a diamond lattice. This condition is valid for 60^o piles but not necessarily for a 30^o pile. Thus we perform different simulations with a 30^o pile on a bumpy bottom, see Fig. 18, with $L_1 = 19$ and *change* the contact network from the regular diamond case by increasing or decreasing the separation of the fixed particles in row $M = 0$. The centers of the particles in the lowermost row are separated by a distance $d_0(1 + c)$, with the c values $c = 1/15$, 0, -1/750, and -1/150. In Fig. 19(a) and (c) the vertical and horizontal components of the stress tensor are plotted, and in Fig. 19(b) and (d) the contact network and the principal axis of the stress tensor, respectively are displayed. The interesting result is that the vertical stress in Fig. 19(a) has a dip for negative c values, the depth of which increases with increasing magnitude of c, see Liffman et al. (1994), Luding (1997). The horizontal stress in Fig. 19(c) is much larger for negative c as for positive c.

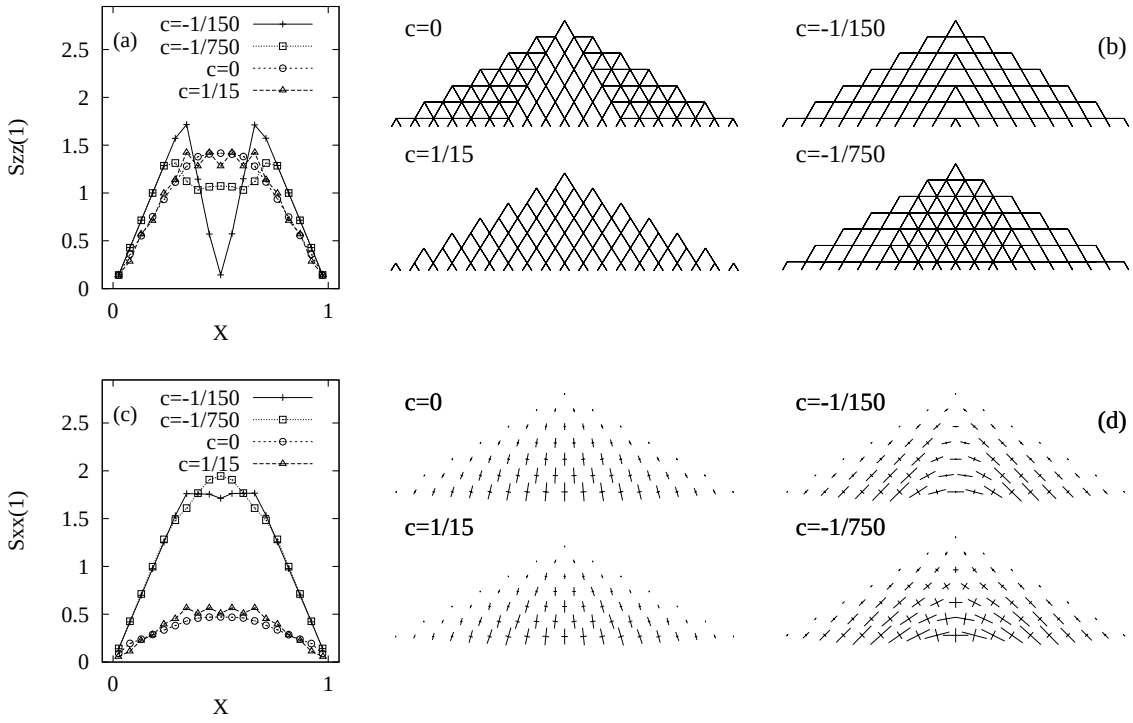

Figure 19: (a) Dimensionless vertical stress $S_{zz}(1)$, in row $M = 1$, vs. dimensionless horizontal coordinate $X = x/l$ for a 30^o pile with bumpy bottom and $L_1 = 19$. The immobile particles in row $M = 0$ are separated by a distance $d_0(1 + c)$, i.e. are sqeezed together for negative c or separated for positive c. (b) The contact networks for the corresponding systems. (c) Horizontal stress $S_{xx}(1)$, vs. X. (d) The principal axis of the stress tensor for the corresponding systems, from Luding (1997).

From Fig. 19(b) we observe that the assumption of a perfect diamond lattice for the contacts is true only for $c = 1/15$, i.e. wide separation of the particles. The vertical stress $S_{zz}(1)$ has a zig-zag structure that we relate to the steps at the surface of a 30^o pile. For the naively used $c = 0$ and also for small negative $c = -1/750$ we have a contact network with regions of coordination number 4 and 6, corresponding to the triangular or the diamond contact network. For sqeezed bottom particles, i.e. $c = -1/150$, the contact network is again a diamond lattice, but the orientation is tilted outwards from the center. From Fig. 19(d) we obtain arching for negative c and no arching for positive c. Evidently, a tilted diamond lattice is necessary for an arch to form in this situation.

In Fig. 20(a) we present for the simulations from Fig. 19 the angle $\phi(1)$, see Eq. (20) about which the major principal axis is rotated from the horizontal in counterclockwise direction. For $c < 0$ we observe a constant angle in the outer part – consistent with the fixed principal axis (FPA) theory by Wittmer et al. (1996) – and a transition region in the center. We observe FPA only for negative c when we also find arching. In contrast, for $c \geq 0$ we observe a slow continuous variation of $\phi(1)$ over the whole pile. In Fig. 20(b) we plot the ratio of the principal axis $s = S_{\min}/S_{\max}$ and observe an almost constant value in the outer region of the pile, whereas in the inner part the ratio is strongly c dependent. From a detailed comparison of the contact network and the stress tensor we may correlate several facts: First, the ratio of the principal axis, s, seems to determine whether the contact network is a triangular or a diamond structure, the latter with one open contact. For $c = 0$ and for $c = -1/750$ the triangular contact network is formed if s is large. Second, the direction of the diamonds is correlated to ϕ, i.e. the tilted diamond lattice (for negative c) is observed if the major axis is tilted sufficiently from the horizontal.

8.3 Polydisperse Particles

Starting from a monodisperse 30^o pile with bumpy bottom and $L_1 = 97$, we change the particle size of each particle slightly to the diameter $d_i = d_0(1 + r_d^i)$, where r_d^i is a random number homogeneously

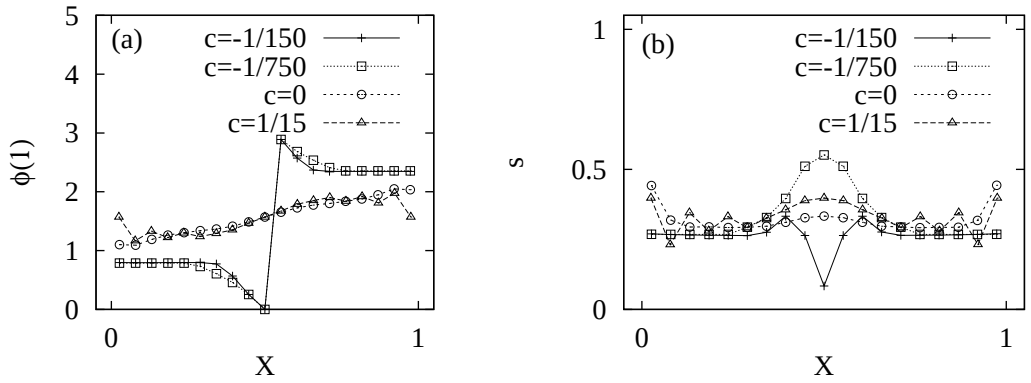

Figure 20: (a) The angle of the major principal axis of the stress, $\phi(1)$, in row $M = 1$ vs. X, from the simulations in Fig. 19, from Luding (1997). (b) The ratio $s = S_{\min}/S_{\max}$ of the principal stresses plotted against X from the simulations in (a).

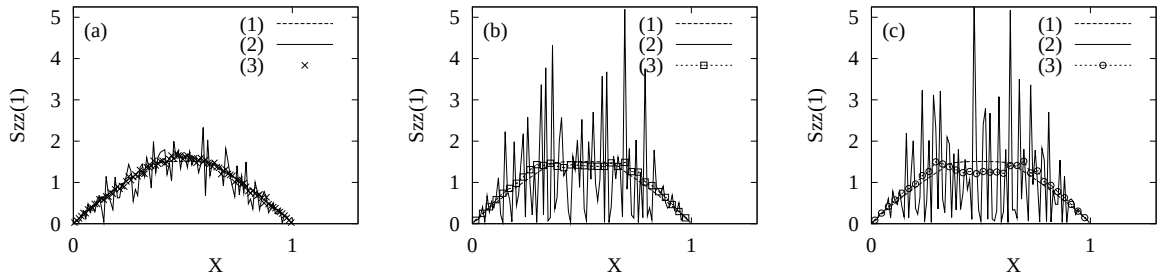

Figure 21: Dimensionless vertical stress $S_{zz}(1)$, in row $M = 1$, vs. X for a 30^o pile with bumpy bottom and $L_1 = 97$ from Luding (1997). The particle diameter is homogeneously distributed in the interval $[d_0(1-r/2), d_0(1+r/2)]$. The values of r_d are $r_d = 2/3000$ (a), $r_d = 2/300$ (b), and $r_d = 1/30$ (c). The dashed line gives the result with no disorder $r_d = 0$ and $L_1 = 97$. The solid line gives the result of one representative run and the dotted line with symbols correspond to an average over 40 runs for (a), or 100 runs and three particles for (b) and (c).

distributed in the interval $[-r_d/2, r_d/2]$. We present the vertical stress in Fig. 21, for simulations with $r_d = 2/3000$ (a), $2/300$ (b), and $1/30$ (c). We plot the result of one run (solid line) and compare it with the monodisperse case (dashed line) and the average over 40 runs (a) or 100 runs (b) and (c) (symbols). The fluctuations in stress increase with increasing r_d. In fact we observe fluctuations much larger than the total stress for the monodisperse pile. With increasing r_d the shape of the averaged vertical stress changes in the center from a hump [see $r_d = 2/3000$], to a dip [see $r_d = 1/30$]. The averaged stress in Fig. 21(c) is similar to the stress obtained (after many averages) from a cellular automaton model for the stress propagation in the presence of randomly opened contacts, see also Hemmingsson et al. (1997).

In Fig. 22 we give the contact network of one run as presented in Fig. 21(c). The line thickness indicates the magnitude of forces active at a contact. Each line represents the normal direction of one contact and each particle center is thus situated at the meeting point of several lines. Note that some particles inside the pile have no contacts to their above neighbors, i.e. they are situated below a small arch. Measuring the probability distribution of the forces, we observe results in agreement with the theoretical predictions by Liu et al. (1995), and the numerical findings by Radjai et al. (1996), at least for large forces. The probability to find large stresses decreases exponentially with the magnitude of the stress and is greater for $r_d = 1/30$ than for $r_d = 2/300$, corresponding to stronger fluctuations.

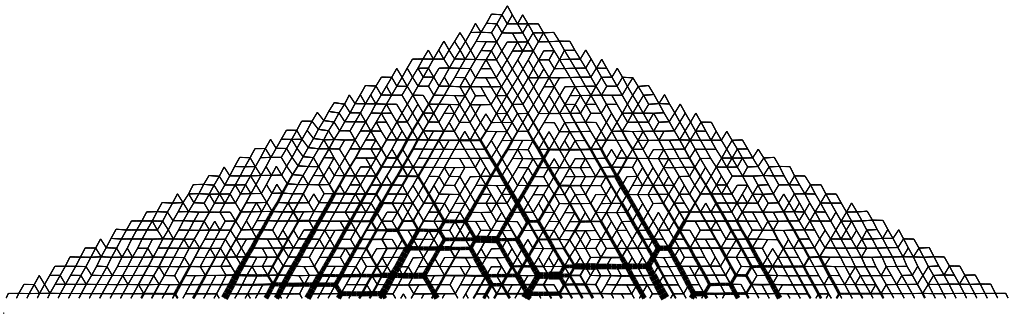

Figure 22: Contact network of one pile from Fig. 21(c). The line thickness indicates the magnitude of the contact force, from Luding (1997).

8.4 The role of the contact network

In this section, we present simulations of static 2D piles made of almost monodisperse spheres. With this simplified model we reproduce theoretical predictions which were based on the assumption of a homogeneous contact network in the whole pile and perfectly rigid particles. Furhtermore, we report phenomena and stress states which could not be observed with a given contact network.

One fact is that arching and the dip in the vertical stress at the bottom are not necessarily due to solid friction, see Liffman et al. (1994), Edwards and Mounfield (1996). If the contact network varies within the pile, stresses different from the theoretical predictions on a regular network are observed. Correlated to arching, the orientation of the stress tensor is fixed – at least in the outer part – and the contact network is symmetric about the center but not translational invariant when changing from the left to the right half of the pile. The orientation of the major principal axis and the ratio of the two principal values of the stress tensor are correlated with the structure of the contact network. We observe diamond lattices, either vertical or tilted by 60 degrees outward from the center, if the major principal stress is almost vertical or tilted outwards, respectively. However, if the major and minor principal axes are comparable in magnitude a triangular lattice with closed contacts is obtained, rather than a diamond lattice. Together with the tilted contact network, i.e. strongly tilted principal axis, we evidence in some cases arching and a small vertical stress beneath the center of the pile. If the contact network is tilted outwards, stresses are preferentially propagated outwards; this may be regarded as a reason for arching and for the dip.

Randomly varying the size of the particles, we find that already tiny polydispersities destroy the regular contact network. Due to the small fluctuations in particle size the particles are still positioned on a triangular lattice even when the contacts are randomly open. For a random network we also find the so called stress chains, i.e. selected paths of large stresses, and the stress fluctuations are larger or of the order of the mean stress. The stress chains - or better the stress network - is also disordered. When averaging over many realizations of the stress network a dip in the vertical stress at the bottom is obtained if the size fluctuations are sufficiently large. Note that the transition from a homogeneous network to the stress chains is controlled by the ratio of particle overlap δ and size fluctuation $r_d d$ but not by the size fluctuations alone. The particle overlap is a function of the particle stiffness and of the local stress $\delta \propto \sigma / k_n$.

Since we were able to find most of the phenomenology expected in a sandpile in an oversimplified regular model system without friction, we conclude that the role of the contact network (or the fabric) is eminent. Nevertheless, friction and small polydispersity may play a different role in more general situations with physical sandpiles.

9 Plastic deformation and shear bands in dense packings

The plastic yield criterion of granular material is quite different from that of metals because, on one hand, it linearly depends on pressure (Mohr-Coulomb) and, on the other hand, because under shear a dilatation along an angle ψ is observed. The yield plane of plasticity is well described by the relation, see Byerlee (1968)

$$\tau = c + \tan(\phi)\sigma_n \tag{23}$$

where τ and σ_n are the shear and the normal stresses on the yield plane and the material constants ϕ and c are the "friction angle" and the cohesion, respectively. In general, the plasticity is "non-associate", i.e. the angle of dilatancy ψ under shear is different from ϕ.

Using an explicit Lagrangian technique similar to FLAC (Fast Lagrangian Analysis of Continua), see Cundall (1989) an elasto-plastic medium was used by Poliakov et al. (1994), Poliakov and Herrmann (1994). The horizontal boundaries were pulled apart with small, constant velocity $V_{\rm bc}$ while the vertical boundaries were moved towards each other with the same velocity $V_{\rm bc}$, so as to assure volume conservation. The yield condition of Eq. (23) was used. Besides the above mentioned material constants c, ϕ and ψ one can also vary the elastic moduli or Lamé constants λ and μ. The simulations are performed on a grid which in its undeformed state is a square lattice of unit lattice constant with one additional diagonal resulting thus in a triangulation. The numerical technique has an intrinsic time step Δt. Measuring length in units of the grid spacing and time in units of Δt, the velocity $V_{\rm bc} = 10^{-5}$ is imposed per grid element.

In Fig. 23 we see snapshots from the evolution of the system with different mesh (lattice) sizes L but the same physical parameters. These results are shown after such a long time that the overall number of shear bands does not change with time (however the positions and activities of single shear zones is not constant). The local changes of the second invariant of the strain rate: $e = \dot{\varepsilon}_{\rm II} = \sqrt{(\dot{\varepsilon}_{\rm xx} - \dot{\varepsilon}_{\rm yy})^2/4 + \dot{\varepsilon}_{\rm xy}^2}$ determine the grey scale in Fig. 23.

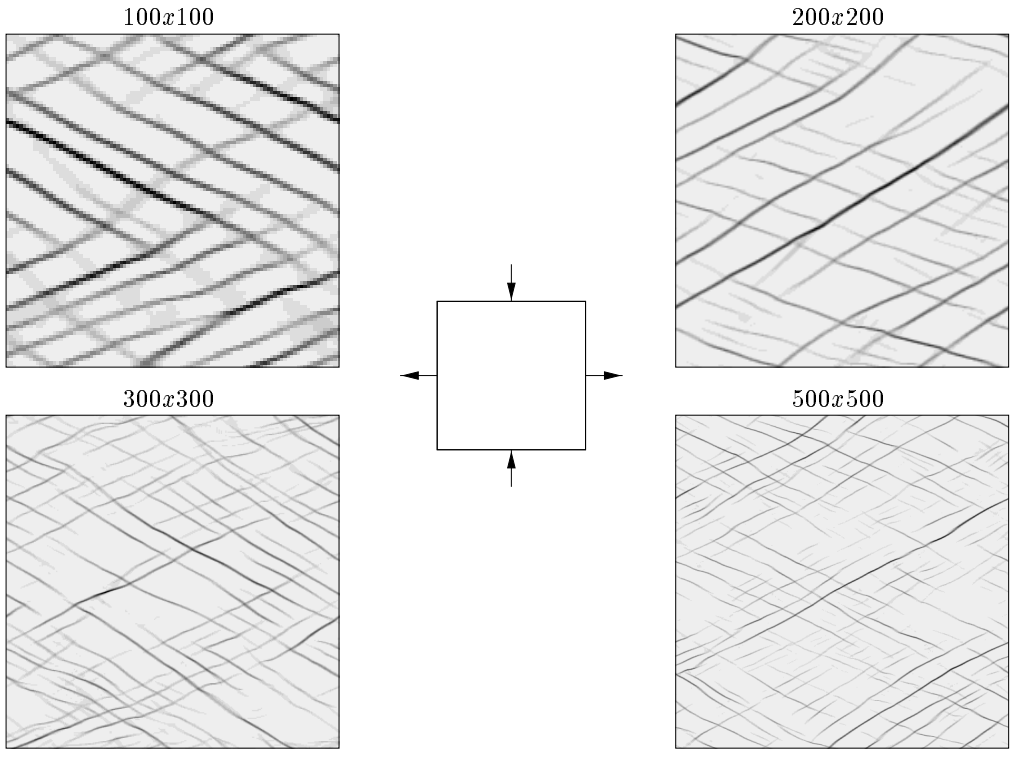

Figure 23: Snapshot of the second invariant e of the strain rate for systems of different size (a) 50x50 (b) 100x100 (c) 200x200 (d) 300x300 for $\phi = 40^o$, $\psi = 0$, $c = 0$, $\lambda = \mu$, Poisson ratio $\nu = 0.25$ and $R = pV_s/(\mu V_{\rm bc}) = 10^{-9}$ with pressure p and velocity of sound V_s, from Poliakov et al. (1994), Poliakov and Herrmann (1994). The central insert gives the direction of the wall motion.

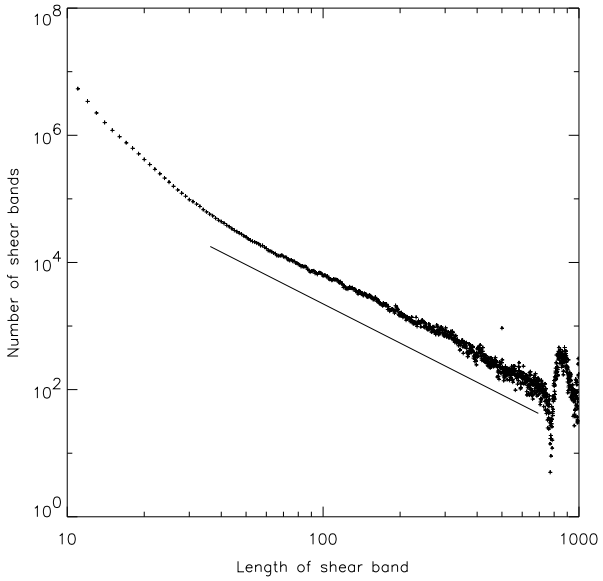

Figure 24: Log-log plot of the length distribution, measured in grid spacing, for a system of size 300 x 300 for the same physical parameters as in Fig. 23, from Poliakov et al. (1994), Poliakov and Herrmann (1994). The line indicates a slope of $m = 2.1$

This means that the dark regions correspond to strong changes either in the direction or in the magnitude of the motion of the material. The white regions are elastic. We see that spontaneously shear bands are formed in which the plastic deformation occurs. These bands form an angle $45° - \phi/2 < \theta < (45° - \psi/2)$ with respect to the horizontal which is consistent with a bifurcation theory, see Vermeer (1990), Vermeer and de Borst (1984). They have varying length and their position changes in time. Since our initial setup was completely homogeneous the random positions of the shear bands are due to minute effects in the round-off of the floating point numbers in the computer.

It has been observed that the pattern formed by the shear bands essentially only depends on the dimensionless parameter $R = pV_s/(\mu V_{\rm bc})$ where p is the confining pressure, V_s the velocity of sound, μ the Lamé constant and $V_{\rm bc}$ the externally imposed velocity of the boundary. This can be checked numerically by varying p, the elastic modulus and the size of the sample. With decreasing R shear bands are located closer to each other. The scale invariance of the shear bands can be analyzed by changing the lattice size L or equivalently the resolution of the system. The geometrical fractal dimension of the shear band network is $d_0 = 1.82 \pm 0.1$ for $R = 10^{-9}$. The same result is obtained from the box-counting analysis of a single picture with the highest resolution, see Poliakov et al. (1994), Poliakov and Herrmann (1994).

The spontaneous appearance of a fractal set of shear bands starting out from a rather homogeneous situation suggests the existence of self-organized criticality, see Bak et al. (1987). Each shear band might be seen as a single internal avalanche on which the system can release stresses through larger displacements. Let us also look at the distribution of the length of shear bands. Numerically it can be obtained using a search routine like the "burning" algorithm, see Herrmann et al. (1984). In Fig. 24 we see a log-log plot of this distribution. For lengths smaller than the width of the bands the data are not useful. Beyond that we see a power-law decay with an exponent of $m = 2.1 \pm 0.2$. This value is in reasonable agreement with length distributions measured on sand, see Sornette et al. (1991).

There is some resemblance between fracture of rocks and shear bands in granular media. It is, however, important to point out a crucial difference between the two: for cracks the most stressed regions are at the tips while the shear bands have their strongest strain rates in the center.

As another example of how a powerful tool discrete simulations can be, we present in Fig. 25 an example of shear banding under plane shear. The horizontal shear band becomes visible, when one marks those particles which rotated most (greyscale in the figure).

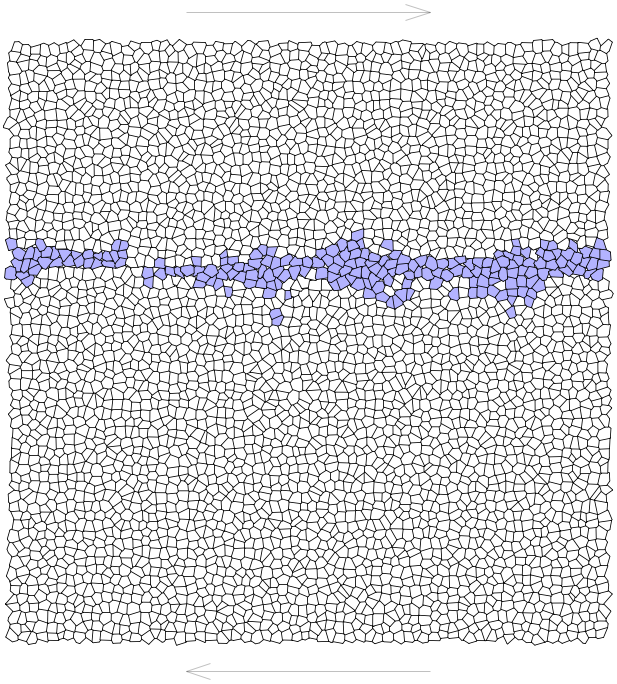

Figure 25: Dense array of polygonal particles under shear in horizontal direction. At top and bottom the system is connected to rigid plates that shear against each other at fixed velocity in the direction indicated by the arrows. A constant normal (vertical) load is imposed and in the horizontal direction periodic boundaries are used. The greyscale indicates those particles which rotated away from their initial orientation by more than 3^o, from Tillemans and Herrmann (1995).

10 Summary and Conclusion

The analogy of molecular systems for which Molecular Dynamics simulations were originally conceived gave us the incentive to describe within a thermodynamic formalism the fluctuations arising from the constant flux and dissipation of energy that drives the kinematic behavior of a granular material. By separating the dissipative degrees of freedom (friction and plasticity) from the conservative ones (translation, rotation, elasticity) we define a "granular ensemble" coupled to a "dissipation bath" which is in fact the one in which experimental and numerical measurements are usually performed. With a rather simple description of a granular medium as an ensemble of inelastic spherical particles with shear friction we have shown that many interesting rheological properties can be reproduced. Various types of convection can occur on a vibrating plate which are strongly influenced by the influence of the walls. In dilute vibrated systems, we observe density and velocity distributions differing from the classical case of an elastic gas. Vibration can also lead to size segregation as connected to convection inside the bulk. When materials flow inside silos, density waves appear which can be explained as a consequence of dissipation: Due to the inelastic collisions between particles an instability, see Goldhirsch and Zanetti (1993), Savage (1992), tends to form clusters of high density (light regions in Fig. 10). These clusters self-organize into a critical state giving a power law spectrum of the pressure on the walls. The density dependence of the viscosity as predicted by the kinetic gas theory builds up waves of low density (dark regions in Fig. 10). We see that simply introducing dissipation to a gas of particles produces several phenomena, that occur simultaneously in granular materials. Looking in much more detail at the reasons for the density fluctuations, we find pressure waves causing dynamic arches which allow "cracks" to open. In regions of large anisotropic stresses the material is not necessarily frustrated. The surfaces are coupled via friction when the confining stress is large and sliding occurs when the stress is small. This may lead to visible spin-order in packings of identical spheres. When examining the growth of a sandpile made of two different species, we find stratification, i.e. the segregation of the two particle species on lines parallel to the free surface. We reproduce this type of pattern with a simple numerical model that accounts for dissipation, friction, and particle inertia. Inside a sandpile we examined the stress distribution. We correlate the anisotropy and direction of the stress tensor to the contact network of the granular material and evidence arching as a result of

a specific arrangement of the fabric. Already tiny variations in particle-size lead to the stress-chains usually found in polydisperse arrays. This is due to the fact that size-disorder as small as the typical deformation of the grains is sufficient to create overall stress fluctuations with the same statistics as for larger size-disorder. Finally we examined shear zones using a Lagrangian technique for elasto-plastic materials and mentioned a MD method that accounts also for the non-spherical shape of the particles.

We have seen that the appearance of large computer power has pushed very strongly the understanding of granular materials. On the one hand it is now possible to track down simultaneously the trajectories of each individual grain out of millions of particles. Although those numbers are still much too small for most technical applications, a RVE (Representative Volume Element) can be simulated in three-dimensions which is a basic tool to numerically access the constitutive behaviour one would insert into a continuum theory. This kind of micro-macro-approach is crucial for soil mechanics and the study of consolidated granular systems. The new techniques of taking into account realistically millions of particles also allow insight into completely new phenomena. These are completely out of the range of the continuum theory but still of collective nature. Some have been presented in the present review article, like anomalous scaling or size segregation under vibrations, fluctuations in hopper flow, spin self-organization and arching phenomena in pipe flow, and peculiar stress distributions in static granular media.
The rapid evolution of novel algorithms also allows to simulate a much larger number of particles by simplifying the details of the collisions. We have presented in fact several examples of this strategy like the DSMC method or the one-dimensional models for stratification during the growth of a sand pile. Much progress can be expected in making such simplified algorithms more realistic without loosing their descriptive power.
The progress in the understanding of collective phenomena during the past 30 years in statistical physics has also boosted the understanding of granular materials. So, for instance, do critical phenomena give a natural framework in the understanding of the scaling loss of vibrated beds, the intermittency in hopper and pipe flow, avalanche statistics, and the distribution of forces inside a packing. Simple toy models known as self-organized criticality (SOC) give us the basic mechanism that produces the power laws in the spectrum of the density of outflowing hoppers or in the acoustic signal of a deformed packing. Modern concepts in physics, as non-linear dynamics and disordered systems, are very useful to understand better the dynamics of the compaction of a granular packing under vibrations.

The present situation allows to predict that the evolution will go on and a more and deeper understanding of the strange effects in granular systems will be achieved within the next decade by the fruitful collaboration of engineers and physicists.

Achnowledgements

We thank E. Clément, J. Duran, E. Flekkøy, J. Gallas, Y. Grasselli, J. Lee, S. Melin, G. Peng, A. Poliakov, T. Pöschel, J. Rajchenbach, M. Rimmele, G. Ristow, and S. Sokołowski, our collaborators on results presented in this paper. Furhtermore, we acknowledge the support of the DFG, SFB 382 (A6).

References

1. Ahmad K, Smalley IJ (1973) Observation of particle segregation in vibrated granular systems. Powder Technol., 8:69.
2. Alexander FJ, Garcia AL, Alder BJ (1995) A consistent Boltzmann algorithm. Phys. Rev. Lett., 74:5212.
3. Allen MP, Tildesley DJ (1987) Computer Simulation of Liquids. Oxford University Press, Oxford.
4. Alonso JJ, Herrmann HJ (1996) On the shape of the tail of a sand pile. Phys. Rev. Lett., 76:4911–4914.
5. Alonso JJ, Hovi JP, Herrmann HJ (1997) Model for the calculation of the angle of repose from the microscopic grain properties. submitted.

6. Athey JD, Cutress JO, Pulfer RF (1966) X-ray investigation on flowing powders. Chem. Eng. Sci., 21:835.
7. Bak P, Tang C, Wiesenfeld K (1987) Self-organized criticality: An explanation of $1/f$ noise. Phys. Rev. Lett., 59(4):381–384.
8. Bardet JP (1994) Observations on the effects of particle rotations on the failure of idealized granular materials. Mechanics of Materials, 18:159–182.
9. Bardet JP, Proubet J (1991) A numerical investigation of the structure of persistent shear bands in granular media. Geotechnique, 41(4):599–613.
10. Bashir YM, Goddard JD (1991) A novel simulation method for the quasi-static mechanics of granular assemblages. J. Rheol., 35(5):849–885.
11. Bathurst RJ, Rothenburg L (1988) Micromechanical aspects of isotropic granular assemblies with linear contact interactions. J. Appl. Mech., 55:17.
12. Baxter GW, Behringer RP (1990) Cellular automata models for granular flow. Phys. Rev. A (Rapid Communication), 42(2):1017.
13. Baxter GW, Behringer RP (1991) Cellular automata models for the flow of granular materials. Physica D, 51:465.
14. Baxter GW, Behringer RP, Fagert T, Johnson GA (1989) Pattern formation in flowing sand. Phys. Rev. Lett., 62(24):2825.
15. Baxter GW, Leone R, Behringer RP (1993) Experimental test of time scales in flowing sand. Europhys. Lett., 21(5):569–574.
16. Behringer RP, Jenkins JT, editors (1997) Powders & Grains 97. Balkema, Rotterdam.
17. Bernu B, Mazighi R (1990) One-dimensional bounce of inelastically colliding marbles on a wall. J. Phys. A: Math. Gen., 23:5745.
18. Bird GA (1994) Molecular Gas Dynamics and the Direct Simulation of Gas Flows. Clarendon, Oxford.
19. Blair-Fish P, Bransby P (1973) Flow patterns and wall stresses in a mass-flow bunker. J. Eng. for Industry, 95:17.
20. Bouchaud JP (1994) Statics and dynamics of sandpiles: some phenomenological ideas. In Bardhan KK, Chakrabarti BK, Hansen A, editors, Lecture Notes in Physics, volume Non Linearity and Breakdown in Soft Condensed Matter, pages 47–53. Springer-Verlag, Berlin.
21. Bouchaud JP, Cates ME, Claudin P (1995) Stress distribution in granular media and nonlinear wave equation. J.Phys.I, 5:639–656.
22. Brennen CE, Ghosh S, Wassgren C (1993) Vertical oscillation of a bed of granular material. In Thornton C, editor, Powders & Grains 93, Rotterdam. Balkema.
23. Bridgwater J (1976) Fundamental powder mixing mechanisms. Powder Technol., 15:215.
24. Brown RL (1939) The fundamental principles of segregation. The Institute of Fuel, 13:15–19.
25. Brown RL, Richards JC (1970) Principles of Powder Mechanics. Pergamon Press, Oxford.
26. Buchholtz V, Pöschel T (1994) Numerical investigations of the evolution of sandpiles. Physica A, 202:390.
27. Buchholtz V, Pöschel T, Tillemans HJ (1995) Simulation of rotating drum experiments using non-circular particles. Physica A, 216:199.
28. Byerlee JD (1968) Brittle-ductile transition in rocks. J. Geophys. Res., 73:4741.
29. Campbell CS (1990) Rapid granular flows. Annu. Rev. Fluid Mech., 22:57.
30. Campbell CS, Brennen CE (1985) Computer simulation of granular shear flows. J. Fluid. Mech., 151:167.
31. Caram H, Hong DC (1991) Random-walk approach to granular flows. Phys. Rev. Lett., 67(7):828.
32. Chen W (1995) Experimental observation of self-localized structure in granular material. Phys. Lett. A, 196:321.

33. Christensen K, Corral A, Frette V, Feder J, Jossang T (1996) Tracer dispersion in a self-organized critical system. Phys. Rev. Lett., 77(1):107–110.

34. Clément E, Duran J, Rajchenbach J (1992) Experimental study of heaping in a two-dimensional "sandpile". Phys. Rev. Lett., 69(8):1189.

35. Clément E, Luding S, Blumen A, Rajchenbach J, Duran J (1993) Fluidization, condensation and clusterization of a vibrating column of beads. Int. J. of Mod. Phys. B, 7(9 & 10):1807–1827.

36. Clément E, Rajchenbach J (1991) Fluidization of a bidimensional powder. Europhys. Lett., 16(2):133.

37. Cundall PA (1974) Report ad/a - 001 602. Technical report, U.S. Nat. Tech. Information Service, Springfield VA.

38. Cundall PA (1989) Numerical experiments on localization in frictional materials. Ingenieur-Archiv, 59:148–159.

39. Cundall PA, Strack O. DL (1979) A discrete numerical model for granular assemblies. Géotechnique, 29(1):47–65.

40. Cutress O, Pulfer RF (1967) X-ray investigation on flowing powders. Powder Technol., 1:213.

41. Désérable D, Martinez J (1993) Using a cellular automaton for the simulation of flow of granular media. In Thornton C, editor, Powders & Grains 93, page 345, Rotterdam. Balkema.

42. Devillard P (1990) Scaling behaviour in size segregation ("Brazil Nuts") J. Phys. France, 51:369.

43. Dinkelacker F, Hübler A, Lüscher E (1987) Pattern formation of powder on a vibrating disc. Biol. Cybern., 56:51.

44. Dippel S, Luding S (1995) Simulations on size segregation: Geometrical effects in the absence of convection. J. Phys. I France, 5:1527.

45. Dobry R, Ng TT (1989) Discrete modelling of stress-strain behaviour of granular media at small and large strains. In Proc. 1st U.S. Conf. on Discrete Element Meth., Nat. Sci. Found., Washington DC.

46. Douady S, Fauve S, Laroche C (1989) Subharmonic instabilities and defects in a granular layer under vertical vibrations. Europhys. Lett., 8(7):621.

47. Drake TG (1990) Structural features in granular flows. J. of Geophysical Research, 95(B6):8681–8696.

48. Drescher A, de Josselin de Jong G (1972) Photoelastic verification of a mechanical model for the flow of a granular material. J. Mech. Phys. Solids, 20:337–351.

49. Du Y, Li H, Kadanoff LP (1995) Breakdown of hydrodynamics in a one-dimensional system of inelastic particles. Phys. Rev. Lett., 74(8):1268–1271.

50. Duran J, Mazozi T, Clément E, Rajchenbach J (1994) Size segregation in a two-dimensional sandpile: convection and arching effects. Phys. Rev. E, 50(6):5138–5141.

51. Duran J, Mazozi T, Luding S, Clément E, Rajchenbach J (1996) Discontinuous decompaction of a falling sandpile. Phys. Rev. E, 53(2):1923.

52. Duran J, Rajchenbach J, Clément E (1993) Arching effect model for particle size segregation. Phys. Rev. Lett., 70(16):2431–2434.

53. Edwards SF (1991) Dynamics of complex flow. J. Stat. Phys., 62:889.

54. Edwards SF, Mounfield CC (1996) A theoretical model for the stress distribution in granular matter. III: Forces in sandpiles. Physica A, 226:25.

55. Edwards SF, Oakeshott R. BS (1989a) Theory of powders. Physica A, 157:1080.

56. Edwards SF, Oakeshott R. BS (1989b) The transmission of stress in an aggregate. Physica D, 38:88–92.

57. Ehrichs EE, Jaeger HM, Karczmar GS, Knight JB, Kuperman V, Nagel SR (1995) Granular convection observed by magnetic resonance imaging. Science, 267:1632–1634.

58. Evesque P, Rajchenbach J (1989) Instability in a sand heap. Phys. Rev. Lett., 62(1):44.

59. Faraday M (1831) On a peculiar class of acoustical figures; and on certain forms assumed by groups of particles upon vibrating elastic surfaces. Philos. Trans. R. Soc. London, 52:299.

60. Flekkoy EG, Herrmann HJ (1993) Lattice Boltzmann models for complex fluids. Physica A, 199:1.

61. Foerster SF, Louge MY, Chang H, Allia K (1994) Measurements of the collision properties of small spheres. Phys. Fluids, 6(3):1108–1115.

62. Frette V, Christensen K, Malthe-Sorenssen A, Feder J, Jossang T, Meakin P (1996) Avalanche dynamics in a pile of rice. Nature, 379:49–51.

63. Gallas J. AC, Herrmann HJ, owski SS (1992a) Molecular dynamics simulation of powder fluidization in two dimensions. Physica A, 189:437.

64. Gallas J. AC, Herrmann HJ, Pöschel T, owski SS (1996) Molecular dynamics simulation of size segregation in three dimensions. J. Stat. Phys, 82:443.

65. Gallas J. AC, Herrmann HJ, Sokołowski S (1992b) Convection cells in vibrating granular media. Phys. Rev. Lett., 69(9):1371.

66. Gervois A, Bideau D (1992) Some geometrical properties of two-dimensional hard disk packings. In Bideau D, editor, Disorder and Granular Media, Amsterdam. North Holland.

67. Goddard JD (1986) Microstructural origins of continuum stress fields - a brief history and some unresolved issues. In DeKee D, Kaloni PN, editors, Recent Developments in Structered Continua. Pitman Research Notes in Mathematics No. 143, page 179, New York. Longman, J. Wiley.

68. Goddard JD (1990) Nonlinear elasticity and pressure-dependent wave speeds in granular media. Proc. R. Soc. Lond. A, 430:105.

69. Goldhirsch I, Zanetti G (1993) Clustering instability in dissipative gases. Phys. Rev. Lett., 70(11):1619–1622.

70. Goldshtein A, Shapiro M (1995) Mechanics of collisional motion of granular materials. Part 1. General hydrodynamic equations. J. Fluid Mech., 282:75–114.

71. Grabinsky M (1992) Qunatifying rock stress and evaluating its significance in the geomechanical design of underground mines. PhD thesis, Univ. of Toronto.

72. Grasselli Y, Herrmann HJ (1997) On the angles of dry granular heaps. Physica A, 246:301–312.

73. Grasselli Y, Herrmann HJ (1998) Experimental study of granular stratification. Granular Matter, 1(1) in press.

74. Haff PK (1983) Grain flow as a fluid-mechanical phenomenon. J. Fluid Mech., 134:401–430.

75. Haff PK, Werner BT (1986) Computer simulation of the mechanical sorting of grains. Powder Technol., 48:239–245.

76. Hanes DM, Inman DL (1985) Observations of rapidly flowing granular-fluid materials. J. Fluid Mech., 150:357.

77. Hansen A, Bideau D, editors (1992) Disorder and Granular Media. North Holland, Amsterdam.

78. Held GA, Solina DH, Keane DT, Haag WJ, Horn P, Grinstein GG (1990) Experimental study of critical-mass fluctuations in an evolving sandpile. Phys. Rev. Lett., 65(9):1120–1123.

79. Hemmingsson J, Herrmann HJ, Roux S (1997) On stress networks in granular media. J. Phys. I, 7:291–302.

80. Herrmann HJ (1993) On the thermodynamics of granular media. J. Phys. II France, 3:427.

81. Herrmann HJ (1995) Simulating granular media on the computer. In Garrido PL, Marro J, editors, 3rd Granada Lectures in Computational Physics, pages 67 – 114. Springer, Heidelberg.

82. Herrmann HJ, Hong DC, Stanley HE (1984) Backbone and elastic backbone of percolation clusters obtained by the new method of 'burning'. J. Phys. A, 17:L261.

83. Herrmann HJ, Hovi JP, Luding S, editors (1998) Physics of dry granular media - NATO ASI Series, Dordrecht. Kluwer Academic Publishers.

84. Homsy GM, Jackson R, Grace JR (1992) Report of a symposium on mechanics of fluidized-beds. J. Fluid Mech., 236:477.

85. Hong DC (1993) Stress distribution of a hexagonally packed granular pile. Phys. Rev. E, 47(1):760–762.

86. Hong DC, McLennan JA (1992) Molecular dynamics simulations of hard sphere granular particles. Physica A, 187:159.

87. Huntley JM (1993) Vacancy effects on the force distribution in a two-dimensional granular pile. Phys. Rev. E, 48(5):4099–4101.

88. Huthmann M, Zippelius A (1998) Dynamics of inelastically colliding rough spheres: Relaxation of translational and rotational energy. Phys. Rev. E, 56(6):6275–6278.

89. Hutter K, Szidarovszky F, Yakowitz S (1986) Plane steady shear flow of a cohesionless granular material down an inclined plane: A model for flow avalanches. Part II: Numerical results. Acta Mechanica, 65:239–261.

90. Hwang H, Hutter K (1995) A new kinetic model for rapid granular flow. Continuum Mech. Thermodyn., 7:357–384.

91. Issa JA, Nelson RB (1989) Numerical analysis of micromechanical behaviour of granular materials. In Proc. 1st U.S. Conf. on Discrete Element Meth., Nat. Sci. Found., Washington DC.

92. Jaeger HM, Liu C, Nagel SR (1989) Relaxation at the angle of repose. Phys. Rev. Lett., 62(1):40–43.

93. Jaeger HM, Nagel SR (1992) Physics of the granular state. Science, 255:1523.

94. Jaeger HM, Nagel SR, Behringer RP (1996a) Granular solids, liquids, and gases. Reviews of Modern Physics, 68(4):1259–1273.

95. Jaeger HM, Nagel SR, Behringer RP (1996b) The physics of granular materials. Physics Today, 49(4):32–38.

96. Janssen HA (1895) Versuche über Getreidedruck in Silozellen. Zeitschr. d. Vereines deutscher Ingenieure, 39(35):1045–1049.

97. Jenkins JT (1985) Grad's 13-moment system for a dense gas of inelastic spheres. Arch. Rat'l. Mech. Anal., 87:355.

98. Jenkins JT, Cowin SC (1979) Theories for flowing granular materials. In Cowin SC, editor, Mechanics Applied to the Transport of Bulk Materials, New York. Am. Soc. Mech. Eng.

99. Jenkins JT, Savage SB (1983) A theory for the rapid flow of identical, smooth, nearly elastic, spherical particles. J. Fluid Mech., 130:187–202.

100. Johnson KL (1989) Contact Mechanics. Cambridge Univ. Press, Cambridge.

101. Jullien R, Meakin P (1992) Three-dimensional model for particle-size segregation by shaking. Phys. Rev. Lett., 69(4):640.

102. Jullien R, Meakin P, Pavlovitch A (1993) Jullien and meakin and pavlovitch reply. Phys. Rev. Lett., 70(14):2195.

103. Károly A, Kertész J (1994) Hydrodynamic cellular automata for granular media. In Gruber R, Tomassini M, editors, Proc. 6th Joint EPS-APS Int. Conf. of Phys. Comp., Geneva. EPS.

104. Knight JB, Fandrich CG, Lau CN, Jaeger HM, Nagel SR (1995) Density relaxation in a vibrated granular material. Phys. Rev. E, 51(5):3957–3962.

105. Knight JB, Jaeger HM, Nagel SR (1993) Vibration-induced size separation in granular media: The convection connection. Phys. Rev. Lett., 70(24):3728–3731.

106. Kohring GA (1994) Computer simulations of granular materials: the effect of mesoscopic forces. J. Phys. I, 4:1779.

107. Kohring GA, Melin S, Puhl H, Tillemans HJ, Vermöhlen W (1995) Computer simulations of critical, non-stationary granular flow through a hopper. Comput. Methods in Appl. Mechanics and Eng., 124:2273.

108. Kuhn MR, Mitchell JR (1989) Modelling of soil creep with the discrete element method. In Proc. 1st U.S. Conf. on Discrete Element Meth., Nat. Sci. Found., Washington DC.

109. Labous L, Rosato AD, Dave R (1997) Measurements of collision properties of spheres using high-speed video analysis. preprint.

110. Landau LD, Lifshitz EM (1975) Elasticity Theory. Pergamon Press, Oxford.

111. Laroche C, Douady S, Fauve S (1989) Convective flow of granular masses under vertical vibrations. J. Phys., 50:699–706.

112. Lee J (1995) Scaling behavior of granular particles in a vibrating box. Physica A, 219:305–326.

113. Lee J, Cowin SC, Templeton JS (1974) An experimental study of a kinematics of flow through hoppers. Trans. Soc. Rheol., 18:247.

114. Lee J, Herrmann HJ (1993) Angle of repose and angle of marginal stability: Molecular dynamics of granular particles. J. Phys. A, 26:373.

115. Lee J, Leibig M (1994) Density waves in granular flow: a kinetic wave approach. J. Phys. I France, 4:507.

116. Lee M, Dufty JW (1996) Long wavelength instability for uniform shear flow. preprint.

117. Liffman K, Chan D, Hughes BD (1994) On the stress depression under a sandpile. Powder Technol., 78:263–271.

118. Liffman K, Chan D. YC, Hughes BD (1992) Force distribution in a two dimensional sandpile. Powder Technology, 72:255–267.

119. Liu C, Nagel SR (1992) Sound in sand. Phys. Rev. Lett., 68(15):2301–2304.

120. Liu C, Nagel SR, Schecter DA, Coppersmith SN, Majumdar S, Narayan O, Witten TA (1995) Force fluctuations in bead packs. Science, 269:513.

121. Lorig LJ, Brady B. HG (1984) A hybrid computational scheme for excavation and support design in jointed rock media. In Design and performance of underground excavations; ISRM Symposium, page 105, Cambridge, UK. London: British Geotech. Soc.

122. Lubachevsky BD (1991) How to simulate billards and similar systems. J. of Comp. Phys., 94(2):255.

123. Luding S (1994) Models and Simulations of Granular Materials. PhD thesis, Universität Freiburg.

124. Luding S (1995) Granular materials under vibration: Simulations of rotating spheres. Phys. Rev. E, 52(4):4442.

125. Luding S (1996) Langkorn- oder Kurzkornreis? Lawinenstatistik in Reishaufen hängt von der Kornform ab. Physikalische Blätter, 52(3):203.

126. Luding S (1997) Stress distribution in static two dimensional granular model media in the absence of friction. Phys. Rev. E, 55(4):4720–4729.

127. Luding S (1998) Collisions & contacts between two particles. In Herrmann HJ, Hovi JP, Luding S, editors, Physics of dry granular media - NATO ASI Series, Dordrecht. Kluwer Academic Publishers.

128. Luding S, Clément E, Blumen A, Rajchenbach J, Duran J (1994c) Anomalous energy dissipation in molecular dynamics simulations of grains: The "detachment effect". Phys. Rev. E, 50:4113.

129. Luding S, Clément E, Blumen A, Rajchenbach J, Duran J (1994b) The onset of convection in molecular dynamics simulations of grains. Phys. Rev. E, 50:R1762.

130. Luding S, Clément E, Blumen A, Rajchenbach J, Duran J (1994a) Studies of columns of beads under external vibrations. Phys. Rev. E, 49(2):1634.

131. Luding S, Clément E, Rajchenbach J, Duran J (1996a) Simulations of pattern formation in vibrated granular media. Europhys. Lett., 36(4):247–252.

132. Luding S, Duran J, Clément E, Rajchenbach J (1996b) Computer simulations and experiments of dry granular media: Polydisperse disks in a vertical pipe. In Proc. of the 5th Chemical Engineering World Congress, San Diego. AIChE.

133. Luding S, Duran J, Clément E, Rajchenbach J (1996c) Segregation of particulate solids: Segregation via convection. Pharm. Technol., 20(8):42–44. see also 20(9)

134. Luding S, Duran J, Clément E, Rajchenbach J (1996d) Simulations of dense granular flow: Dynamic arches and spin organization. J. Phys. I France, 6:823–836.

135. Luding S, Duran J, Mazozi T, Clément E, Rajchenbach J (1996e) Simulations of granular flow: Cracks in a falling sandpile. In Wolf DE, Schreckenberg M, Bachem A, editors, Traffic and Granular Flow, Singapore. World Scientific.

136. Luding S, Herrmann HJ, Blumen A (1994d) Scaling behavior of 2-dimensional arrays of beads under external vibrations. Phys. Rev. E, 50:3100.

137. Luding S, Matuttis HG (1997) The effect of interaction laws on the stresses in frictionless granular media. In Wolf DE, Grassberger P, editors, Friction, Arching and Contact Dynamics, pages 373–376, Singapore. World Scientific.

138. Luding S, Müller M, McNamara S (1998) The validity of "molecular chaos" in granular flows. In Proceedings of the World Congress on Particle Technology, Brighton. Institution of Chemical Engineers. to appear.

139. Makse HA, Herrmann HJ (1998) Microscopic model for granular flows of mixtures. submitted.

140. Matuttis HG (1998) Simulations of the pressure distribution under a two dimensional sand-pile of polygonal particles. accepted.

141. Matuttis HG, Luding S (1997) The effect of particle shape and friction on the stresses in heaps of granular media. In Wolf DE, Grassberger P, editors, Friction, Arching and Contact Dynamics, Singapore. World Scientific.

142. Maw N, Barber JR, Fawcett JN (1976) The oblique impact of elastic spheres. Wear, 38:101.

143. Maw N, Barber JR, Fawcett JN (1981) The role of elastic tangential compliance in oblique impact. J. Lubrication Tech., 103:74.

144. Mazighi R, Bernu B, Delyon F (1994) Steady state of a column of shaked inelastic spheres. Phys. Rev. E, 50:4551.

145. McNamara S, Luding S (1998a) Energy flows in vibrated granular media. preprint.

146. McNamara S, Luding S (1998b) The ratio of translational to rotational kinetic energy in granular media. preprint.

147. McNamara S, Young WR (1992) Inelastic collapse and clumping in a one-dimensional granular medium. Phys. Fluids A, 4(3):496.

148. McNamara S, Young WR (1993) Kinetics of a one-dimensional granular medium in the quasielastic limit. Phys. Fluids A, 5(1):34.

149. McNamara S, Young WR (1996) Dynamics of a freely evolving, two-dimensional granular medium. Phys. Rev. E, 53(5):5089–5100.

150. Mehta A, editor (1994) Granular Matter. Springer, Berlin.

151. Mehta A, Edwards SF (1989) Statistical mechanics of powder mixtures. Physica A, 157:1091.

152. Melo F, Umbanhowar PB, Swinney HL (1994) Transition to parametric wave patterns in a vertically oscillated granular layer. Phys. Rev. Lett., 72(1):172–175.

153. Melo F, Umbanhowar PB, Swinney HL (1995) Hexagons, kinks, and disorder in oscillated granular layers. Phys. Rev. Lett., 75(21):3838–3841.

154. Metcalf TH, Knight JB, Jaeger HM (1997) Standing wave patterns in shallow beds of vibrated granular material. Physica A, 236:202–210.

155. Michalowski RL (1984) Flow of granular material through a plane hopper. Powder Technol., 39:29.

156. Mindlin RD (1949) Compliance of elastic bodies in contact. J. of Appl. Mech., 16:259.

157. Mindlin RD, Deresiewicz H (1953) Elastic spheres in contact under varying oblique forces. J. of Appl. Mech., 20:327.

158. Müller M, Luding S, Herrmann HJ (1997) Simulations of vibrated granular media in 2d and 3d. In Wolf DE, Grassberger P, editors, Friction, Arching and Contact Dynamics, Singapore. World Scientific.

159. Ogawa S (1978) Multitemperature theory of granular materials. In Cowin S, Satake M, editors, Proc. of US-Japan Symp. on Continuum Mechanics and Statistical Approaches to the Mechanics of Granular Media, page 208, Fukyu-kai. Gakujutsu Bunken.

160. Oron G, Herrmann HJ (1997) Exact calculation of force networks in granular media. Phys. Rev. E. cond-mat/9707243.

161. Ouaguenouni S, Roux JN (1997) Arching without friction: a simple model. In Wolf DE, Grassberger P, editors, Friction, Arching and Contact Dynamics, Singapore. World Scientific.

162. Pak HK, Behringer PR (1994) Bubbling in vertically vibrated granular materials. Nature, 371:231–233.

163. Pak HK, Behringer RP (1993) Surface waves in vertically vibrated granular materials. Phys. Rev. Lett., 71(12):1832–1835.

164. Pak HK, van Doorn E, Behringer RP (1995) Effects of ambient gases on granular materials under vertical vibration. Phys. Rev. Lett., 74(23):4643–4646.

165. Peng G, Herrmann HJ (1994) Density waves of granular flow in a pipe using lattice-gas automata. Phys. Rev. E, 49(3):1796.

166. Peng G, Herrmann HJ (1995) Density waves and $1/f$ density fluctuations in granular flow. Phys. Rev. E, 51(3):1745.

167. Peng G, Ohta T (1996) Velocity and density profiles of granular flow in channels using lattice gas automaton. preprint.

168. Peng G, Ohta T (1997) Logarithmic density relaxation in compaction of granular materials. preprint.

169. Poliakov A. NB, Herrmann HJ (1994) Self-organized criticality in plastic shear bands. Geophys. Res. Lett., 21:2143–2146.

170. Poliakov A. NB, Herrmann HJ, Podladchikov YY, Roux S (1994) Fractal plastic shear bands. Fractals, 2:567–581.

171. Pöschel T (1993) Granular material flowing down an inclined chute: A molecular dynamics simulation. J. Phys. II, 3:27.

172. Pöschel T (1994) Recurrent clogging and density waves in granular material flowing through a narrow pipe. J. Phys. I France, 4:499.

173. Pöschel T, Buchholtz V (1993) Static friction phenomena in granular materials: Coulomb law vs. particle geometry. Phys. Rev. Lett., 71(24):3963.

174. Pöschel T, Buchholtz V (1995a) Complex flow of granular material in a rotating cylinder. Chaos, Solitons, and Fractals, 5:1901.

175. Pöschel T, Buchholtz V (1995b) Molecular dynamics of arbitrarily shaped granular particles. J. Phys. I France, 5(11):1431–1455.

176. Pöschel T, Herrmann HJ (1995) Size segregation and convection. Europhys. Lett., 29:123.

177. Pöschel T, Rosenkranz DE (1997) Experimental study of horizontally shaken granular matter - the swelling effect. preprint.

178. Potapov AV, Campbell CS (1996) Propagation of elastic waves in deep vertically shaken particle beds. Phys. Rev. Lett., 77:4760.

179. Pouliquen O, Renaut N (1995) Onset of granular flows on an inclined rough bed: dilatancy effects. preprint.

180. Raafat T, Hulin JP, Herrmann HJ (1996) Density waves in dry granular media falling through a vertical pipe. Phys. Rev. E, 53:4345–4355.

181. Raafat T, Terminassian V, Hulin JP, Herrmann HJ (1997) Pressure analysis for pneumatic instabilities during dry granular flows in vertical pipes. preprint.

182. Radjai F, Jean M, Moreau JJ, Roux S (1996) Force distribution in dense two-dimensional granular systems. Phys. Rev. Lett., 77(2):274.

183. Radjai F, Schäfer J, Dippel S, Wolf D (1997) Collective friction of an array of particles: A crucial test for numerical algorithms. J. Phys. I France, 7:1053.

184. Rajchenbach J (1991) Dilatant process for convective motion in a sand heap. Europhys. Lett., 16(2):149.

185. Rapaport DC (1995) The Art of Molecular Dynamics Simulation. Cambridge University Press, Cambridge.

186. Rátkai G (1976) Particle flow and mixing in vertically vibrated beds. Powder Technol., 15:187.

187. Reynolds O (1885) On the dilatancy of media composed of rigid particles in contact. Philos. Mag. Ser. 5, 50-20:469.

188. Ristow GH (1992a) Molecular dynamics simulations of granular materials on the intel ipsc/860. Int. J. of Mod. Phys. C, 3(6):1281.

189. Ristow GH (1992b) Simulating granular flow with molecular dynamics. J. Phys. I, 2(6):649.

190. Ristow GH (1994) Granular dynamics: A review about recent molecular dynamics simulations of granular materials. In Stauffer D, editor, Annual Reviews of Computational Physics I, Singapore. World Scientific.

191. Ristow GH, Herrmann HJ (1994) Density patterns in two-dimensional hoppers. Phys. Rev. E, 50(1):R5–R8.

192. Ristow GH, Herrmann HJ (1995) Forces on the walls and stagnation zones in a hopper filled with granular material. Physica A, 213:474–481.

193. Rosato AD, Lan Y (1993) Discrete element modeling of vibrating granular beds. In Thornton C, editor, Powders & Grains 93, page 241, Rotterdam. Balkema.

194. Rosato AD, Prinz F, Standburg KJ, , Swendsen R (1986) Monte carlo simulation of particulate matter segregation. Powder Technol., 49:59.

195. Rosato AD, Strandburg KJ, Prinz F, Swendsen RH (1987) Why the Brazil nuts are on top: Size segregation of particulate matter by shaking. Phys. Rev. Lett., 58(10):1038.

196. Savage SB (1979) Gravity flow of cohesionless granular materials in chutes and channels. J. Fluid Mech., 92:53.

197. Savage SB (1992) Instability of unbounded uniform granular shear flow. J. Fluid Mech., 241:109.

198. Savage SB (1993) Disoder, diffusion, and structure formation in granular flows. In Bideau D, editor, Disorder and granular media, page 264, Amsterdam. North Holland.

199. Savage SB (1997) Problems in the statics and dynamics of granular materials. In Behringer RP, Jenkins JT, editors, Powders & Grains 97, pages 185–194. Balkema, Rotterdam.

200. Schäfer J, Dippel S, Wolf DE (1996) Force schemes in simulations of granular materials. J. Phys. I France, 6:5–20.

201. Schick K, Verveen A (1974) $1/f$ noise with a low frequency white noise limit. Nature, 251:599.

202. Shattuck MD, Bizon C, Umbanhowar PB, Swift JB, Swinney HL (1997) 2d vertically vibrated granular media: Experiment and simulation. In Powders & Grains 97, Rotterdam. Balkema.

203. Shinbrot T (1997) Granular patterns: A competition between randomizing impacts and inelastic collisions. preprint.

204. Smid J, Novosad J (1981) Pressure distribution under heaped bulk solids. I. Chem. E. Symposium Series, 63:D3/V/1–12.

205. Sornette A, Davy P, Sornette D (1991) Growth of fractal fault patterns. Phys. Rev. Lett., 65:2266.

206. Taguchi Y (1992) New origin of a convective motion: Elastically induced convection in granular materials. Phys. Rev. Lett., 69(9):1367.

207. Taguchi Y, Takayasu H (1995) A set of hard spheres with tangential inelastic collision as a model of granular matter: $1/f$ fluctuation, non-gaussian distribution, and convective motion. preprint.

208. Tanaka T, Yonemura S, Yashi KK, Tsuji Y (1996) Cluster formation and particle-induced instability in gas-solid flows predicted by the dsmc method. JSME Int. Journal B, 39(2):239–245.

209. Thompson PA, Grest GS (1991) Granular flow: Friction and the dilatancy transition. Phys. Rev. Lett., 67(13):1751.

210. Thornton C, editor (1993) Powders & Grains 93. Balkema, Rotterdam.

211. Thornton C, Randall CW (1988) Applications of theoretical contact mechanics to solid particle system simulation. In Micromechanics of granular media, Amsterdam. Elsevier.

212. Tillemans HJ, Herrmann HJ (1995) Simulating deformations of granular solids under shear. Physica A, 217:261–288.

213. Ting JM, Corkum BT, Kauffman CR, Greco C (1989) Discrete numerical-model for soil mechanics. J. of Geotech. Eng., 115:379.

214. Trollope DH, Burman BC (1980) Physical and numerical experiments with granular wedges. Géotechnique, 30(2):137–157.

215. Umbanhowar PB, Melo F, Swinney HL (1996) Localized excitations in a vertically vibrated granular layer. Nature, 382:793–796.

216. Vermeer PA (1990) The orientation of shear bands in biaxial tests. Géotechnique, 40:223.

217. Vermeer PA, de Borst R (1984) Non-associated plasticity for soil, concrete and rock. Heron, 29:1.

218. Vollmar S, Herrmann HJ (1995) Settling of particles studied by a hydrodynamic cellular automaton for granular media. Physica A, 215:411.

219. Walker J (1982) When different powders are shaken, they seem to have lives of their own. Sc. American, 247(3):166.

220. Walton OR (1993a) Numerical simulation of inclined chute flows of monodisperse, inelastic, frictional spheres. Mechanics of Materials, 16:239–247.

221. Walton OR (1993b) Numerical simulation of inelastic, frictional particle-particle interactions. In Roco MC, editor, Particulate two-phase flow, page 884, Boston. Butterworth-Heinemann.

222. Walton OR (1994) Effects of interparticle friction and particle shape on dynamic angles of repose via particle-dynamics simulation. In Workshop: Mechanics and Statistical Physics of Particulate Materials.

223. Walton OR, Braun R (1986) Viscosity, granular-temperature, and stress calculations for shearing assemblies of inelastic, frictional disks. Journal of Rheology, 30(5):949–980.

224. Walton OR, Braun R (1993) Simulation of rotary-drum and repose tests for frictional spheres and rigid sphere clusters. In DOE/NSF Workshop on Flow of Particulates and Fluids, pages 1–17.

225. Warr S, Hansen JP (1996) Relaxation of local density fluctuations in a fluidized granular medium. Europhys. Lett., 36(8):589–594.

226. Warr S, Huntley JM, Jacques G. TH (1995) Fluidization of a two-dimensional granular system: Experimental study and scaling behavior. Phys. Rev. E, 52(5):5583–5595.

227. Warr S, Jacques G. TH, Huntley JM (1994) Tracking the translational and rotational motion of granular particles: use of high-speed photography and image processing. Powder Technol., 81:41–56.

228. Wassgren CR, Hunt ML, Brennen CE (1997) Investigation of $f/2$ and $f/4$ waves in granular beds subject to vertical, sinusoidal oscillations. In Powders & Grains 97, Rotterdam. Balkema.

229. Williams JC (1976) The segregation of particulate materials: A review. Powder Technol., 15:245.

230. Wittmer JP, Cates ME, Claudin P (1997) Stress propagation and arching in static sandpiles. J. Phys. I, 7:39–80.

231. Wittmer JP, Claudin P, Cates M, Bouchaud JP (1996) An explanation for the central stress minimum in sand piles. Nature, 382:336–338.

232. Wolf DE (1996) Modeling and computer simulation of granular media. In Hoffmann KH, Schreiber M, editors, Computational Physics. Springer, Heidelberg.

233. Wolf DE, Grassberger P, editors (1997) Friction, Arching and Contact Dynamics. World Scientific, Singapore.

234. Zik O, Stavans J, Rabin Y (1992) Mobility of a sphere in vibrated granular media. Europhys. Lett., 17(4):315–319.